UNIVERSITY OF OKLAHOMA

GRADUATE COLLEGE

ABSOLUTE-MAGNITUDE DISTRIBUTIONS AND LIGHT CURVES OF STRIPPED–ENVELOPE SUPERNOVAE

A Dissertation

SUBMITTED TO THE GRADUATE FACULTY

in partial fulfillment of the requirements for the

degree of

Doctor of Philosophy

by
DEAN L. RICHARDSON
Norman, Oklahoma
2004

ABSOLUTE-MAGNITUDE DISTRIBUTIONS AND LIGHT CURVES OF STRIPPED–ENVELOPE SUPERNOVAE

A Dissertation APPROVED FOR THE
DEPARTMENT OF PHYSICS AND ASTRONOMY

BY

_____
David Branch (Chair)

_____
Eddie Baron

_____
Ron Kantowski

_____
William Romanishin

_____
S. Lakshmivarahan

Acknowledgments

I want to thank my committee for their help and advice; especially David Branch and Eddie Baron, for whom I have worked for many years and have learned much about supernovae and scientific research in general.

I would also like to mention the important contributions of Darrin Casebeer and Rollin Thomas to the SUSPECT database. They were there from the start and are responsible for the initial development of the database. Jerod Parrent has also contributed to the database and is continuing to contribute.

I would especially like to thank my family who has always been a great source of support and encouragement. Finally, I would like to dedicate this work to the memory of my mother, Donna L. Richardson.

Contents

List of Figures

Abstract

The supernova data archive, SUSPECT, is presented. It is looked at, and mapped out, from the users point of view. The basic details of the operation of the database are also discussed.

The absolute visual magnitudes of three Type IIb, 10 Type Ib and 13 Type Ic supernovae (collectively known as stripped–envelope supernovae) are studied by collecting data on the apparent magnitude, distance, and interstellar extinction of each event. Weighted and unweighted mean absolute magnitudes of the combined sample as well as various subsets of the sample are reported. The limited sample size and the considerable uncertainties, especially those associated with extinction in the host galaxies, still prevent firm conclusions regarding differences between the absolute magnitudes of supernovae of Type Ib and Ic, and regarding the existence of separate groups of overluminous and normal-luminosity stripped–envelope supernovae. The spectroscopic characteristics of the events of the sample are considered. Three of the four overluminous events are known to have had unusual spectra. Most but not all of the normal luminosity events had typical spectra.

Absolute light curves of stripped–envelope supernovae are collected and compared. They show a wide variety in peak brightness and light–curve width. These differences are reflected in the model parameter values determined. The supernova with the greatest kinetic energy (31×10^{51}erg) and ejected mass ($6.2 M_{\odot}$) in the sample is SN 1998bw. The hypernovae, in general, vary in peak brightness and therefore they vary in nickel mass. Supernova components found in gamma–ray burst afterglow light curves are modeled as well. These

are treated as hypernovae and range in kinetic energy from 6.5 to 25 $\times 10^{51}$erg. Two are found (GRB010921 and GRB011121) to have occurred more than a week before their associated gamma–ray burst.

Chapter 1

Introduction

1.1 Description of the Core–Collapse Process that Triggers Supernovae

For the majority of a star's life it is stable, with the forces governing its behavior in balance at all radii. In the core of the star, hydrogen is fused into helium. The energy released in this process causes an outward gas pressure which supports the weight of the star against collapse. At some point the core will have converted nearly all of its hydrogen into helium and the core will begin to contract. Before the core contracts enough to reach the temperature and density necessary to fuse the helium, the hydrogen in a shell just outside the core will reach the temperature and density necessary to fuse (Iben 1967 [39]). This fusion releases energy that produces an outward gas pressure that causes the hydrogen envelope, which is the vast majority of the star, to expand. The star becomes a giant while its core continues to contract. Eventually, the core will reach the temperature and density necessary for the helium to fuse into carbon and oxygen. This process of producing consecutively heavier elements in the core, and in concentric shells around the core, continues until iron is is reached (see Figure 1.1). The iron core is supported by electron degeneracy pressure.

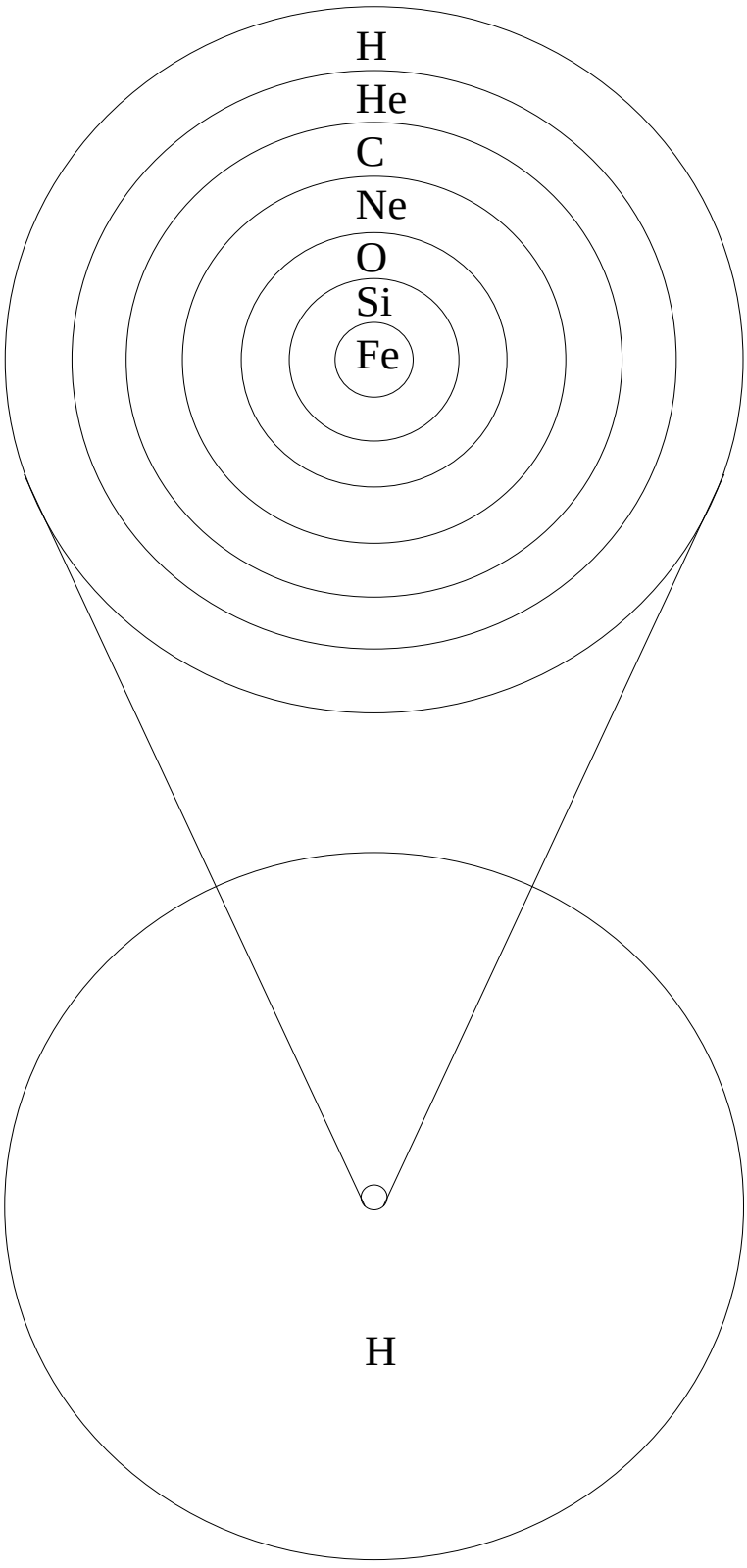

Figure 1.1: The structure of a highly evolved, massive star.

With electron degeneracy there is a limit to how tightly electrons can be packed together[1]. Iron fusion is endothermic, requiring more energy than it produces. As the core contracts, the energy increases and the iron nuclei begin to photodissociate. Electrons are captured by protons, where each capture produces a neutron and a neutrino. Because the electron degeneracy pressure is related to the electron number density ($p \propto n_e^{4/3}$; Clayton 1983 [17]), the decrease in the number of electrons decreases the ability of the electron degeneracy to support the weight of the core and the core collapses.

The density of the core increases beyond nuclear density and rebounds. This begins a shock wave that propagates out through the star. At some point the shock wave stalls. What happens next is not well understood. Some models show that heating from the release of trapped neutrinos could contribute to restarting the shock wave, but this, in itself, would not be enough (Buras et al. 2003 [16]). Other models suggest that a strong magnetic field around a newly formed rotating compact object (such as a neutron star or black hole) could generate a jet capable of, or at least contributing to, restarting the shock wave; similar to what is described by MacFadyen, Woosley & Heger 2001 [54]. While the jet may contribute to restarting the shock wave, it doesn't always make it to the surface; even when the shock wave does. When the shock wave reaches the surface, the star explodes; leaving behind only the neutron core, which is now a neutron star. This is our current understanding of what leads to the explosion of massive stars.

[1]This limit is due to the quantum mechanical effect known as the Pauli exclusion principle.

1.2 The Light Curves of Core–Collapse Supernovae

A light curve is a plot of brightness (flux) versus time. For SN light curves, magnitude is used in place of flux. Magnitude is related to flux by $m = -2.5log_{10}(F) + const.$, where m is the magnitude and F is the flux. As the shock wave reaches the surface there is a very large initial flux of photons. The luminosity reaches a peak in a few hours and then falls sharply as the effect of a decrease in temperature, $L \propto T^4$, outpaces the effect of an increase in the size, $L \propto R^2$, of the ejecta. This is known as the break–out shock and can be seen, if caught early enough, as a spike in the light curve; primarily at ultraviolet wavelengths.

As the photosphere (the radius within which the photons are completely trapped) expands, the luminosity increases. The larger the hydrogen envelope, the less the envelope expands. The shock energy, then goes into heating the envelope instead of expanding the envelope (less pdV work). This heating contributes to the increase in luminosity. The degree to which it contributes, however, depends on the size of the hydrogen envelope.

In the SN explosion, temperatures greater than 5×10^9K are reached in the inner ejecta. At this temperature, explosive nuclear burning converts much of the ejecta into ^{56}Ni. ^{56}Ni (28 protons and 28 neutrons) decays, by electron capture, to ^{56}Co (27 protons and 29 neutrons) emitting a photon and a neutrino. The half life of this process is 6 days. ^{56}Co then decays to ^{56}Fe (26 protons and 30 neutrons) with a half life of 77 days. About 80% of the time the decay is by electron capture, releasing a gamma–ray and a neutrino. The other 20% of the

time the ^{56}Co decays to a gamma–ray, a neutrino and a positron. The positron eventually annihilates with an electron producing a gamma–ray.

As the envelope expands, the photosphere recedes into the ejecta and the luminosity begins to fall. For SNe with large hydrogen envelopes, hydrogen recombination provides enough photons so that the light curve plateaus for awhile. At about one to three months after peak luminosity, depending on whether there is a plateau, there is a transition point where the luminosity becomes primarily determined by the gamma–rays produced in the ^{56}Co decay. These gamma–rays Compton scatter with electrons. The fast moving electrons then interact with ions in the ejecta, slow down and, in doing so, produce optical photons. This produces a steady decline in the late–time SN light curve.

1.3 Classification of Supernovae

In the most basic sense there are only two types of SNe: those with hydrogen in their spectra and those without. The first SN spectra observed showed no signs of hydrogen, the most abundant element in the universe. Later, SNe were discovered whose spectra contained hydrogen features. For this reason SNe without hydrogen in their spectra are called Type I SNe (SNe I) and those with hydrogen in their spectra are called Type II SNe (SNe II). The SNe I break down into three subclasses: SNe Ia, Ib and Ic. SNe Ia have prominent SiII features and no helium. They are not thought to be produced by the core–collapse of massive stars, but rather by the thermonuclear explosion of accreting white dwarfs that have been pushed over their mass limit (the Chandrasekhar limit). SNe Ib have strong helium features and no prominent SiII features. SNe Ic, on

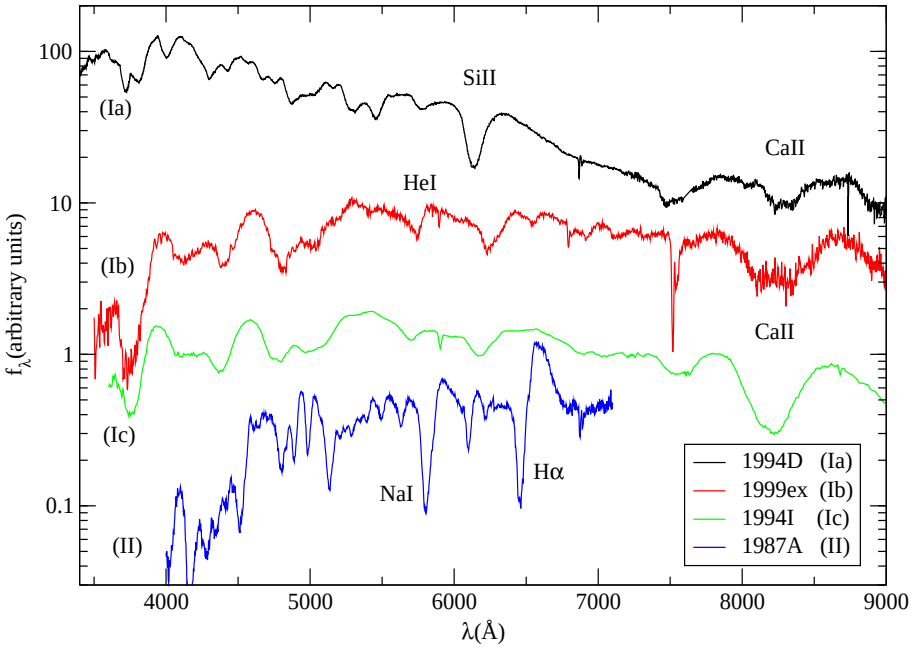

Figure 1.2: Spectra of the various types of SNe.

the other hand, have neither strong SiII or helium features. Both SNe Ib and Ic are found in star forming regions and are quite likely core–collapse SNe of stars that have lost their hydrogen envelopes. A sample of spectra near peak brightness is shown for different SN types in Figure 1.2. All of the spectra in Figure 1.2 are from the SUSPECT database mentioned in Chapter 2 (Ia: SN 1994D [66]; Ib: SN 1999ex [36]; Ic: SN 1994I [19]; II: SN 1987A [72]).

SNe II can be divided into subclasses by both their spectra and their light curves. SNe IIb have hydrogen lines (resembling typical SNe II) at early times and no hydrogen at late times (resembling typical SNe Ib). SNe IIn have narrow lines due to interaction with the slow moving circumstellar medium. The subclasses of SNe II determined by light curves are SNe IIL and IIP. SNe IIP are the plateau SNe mentioned above in §1.2 and the SNe IIL are the SNe II with hydrogen envelopes too small for the light from the recombination of hy-

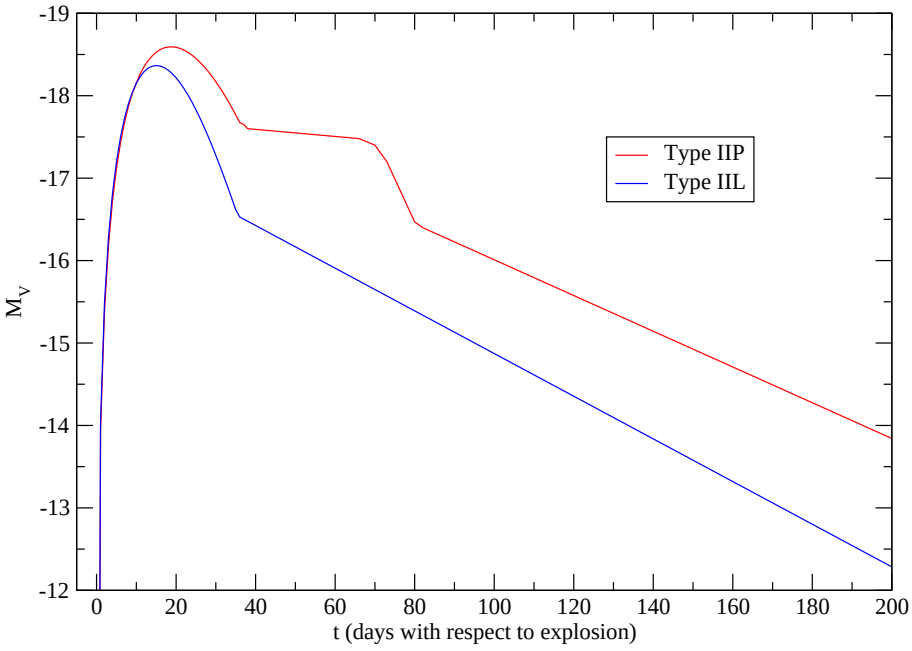

Figure 1.3: Light Curves for SNe IIL and IIP.

drogen to significantly effect the light curve. Schematic light curves are shown for SNe IIL and IIP in Figure 1.3.

1.4 Photometry

Often astronomers observe objects, like SNe, with a filter over the detector. The filter only allows light within a certain wavelength range to enter the detector. The detector then simply counts the photons, giving astronomers a measure of how bright the object is in the filter's wavelength range. The most common filters are B, V, R and I; for blue, visual, red and near infrared, respectively. These filters are represented by filter functions (Bessel 1990 [11]) plotted against a spectrum of SN 1994I in Figure 1.4. The mathematical relation between magnitude and flux is:

$$m_x = -2.5log_{10}\left(\int f(\lambda)S_x(\lambda)d\lambda\right) + ZP_x \tag{1.1}$$

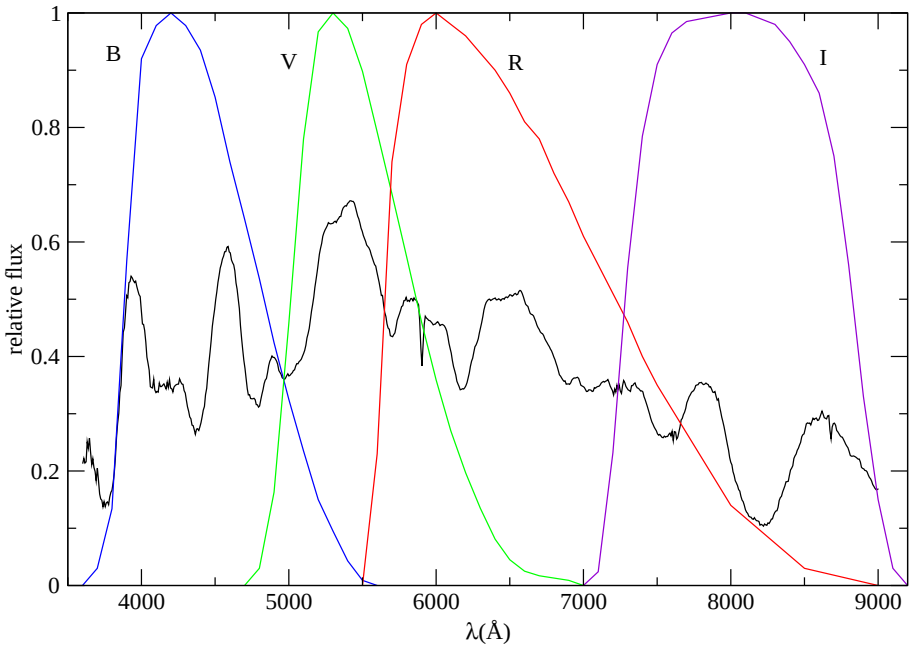

Figure 1.4: Filter functions with a spectrum of SN 1994I

where, $f(\lambda)$ is the SN spectrum, $S_x(\lambda)$ is the filter function and ZP_x is the zero point for filter "x".

When SNe are observed from large cosmological distances their spectra, and therefore their photometry, are altered by the time they reach us. Due to the expanding universe, the wavelength of the light traveling from a distant SN to us expands. This means that we see the light redder than it was when it was emitted. Features in a spectrum of a distant SN are shifted to the red and the flux of light entering the detector though a filter will be different because the spectrum is shifted. B and V filters are most often used for nearby SNe while R and I are most often used for distant SNe. As can be seen in Figure 1.4, the shapes of the filter functions are not the same. A correction must be used to account for the redshift in the spectrum as well as the difference in filter shape. This correction is called a K–correction. The need for a K–correction

is illustrated in Figure 1.5. Figure 1.5a shows a redshifted spectrum with the R filter function. The flux of the spectrum under the filter functions is what is detected. What we want is shown in Figure 1.5b where the spectrum is in the SN's rest frame (unredshifted) and a V filter is used. The K–correction equation used to take the R (or I) magnitude of a redshifted SN to the V (or B) magnitude of the same SN in its rest frame is:

$$\begin{aligned} K_{xy} &= -2.5log_{10}\Big(\frac{\int \mathcal{Z}(\lambda)S_x(\lambda)d\lambda}{\int \mathcal{Z}(\lambda)S_y(\lambda)d\lambda}\Big) \\ &\quad +2.5log_{10}\Big(\frac{\int f(\lambda)S_x(\lambda)d\lambda}{\int f(\lambda)S_y(\lambda(1+z))d\lambda}\Big) - ZP_x + ZP_y, \end{aligned} \tag{1.2}$$

where, "y" is the observed filter (R or I) and "x" is the desired filter (B or V). The spectrum of the SN is $f(\lambda)$. The magnitudes are normalized to Vega. Here the spectrum for Vega is represented by $\mathcal{Z}(\lambda)$. Because the apparent magnitudes of Vega are not exactly zero ($B \neq 0,\ V \neq 0,\ \ldots$) the zero point corrections, ZP_x and ZP_y, need to be added to get the correct calibrations [1]. The redshift is defined as $z \equiv (\lambda_o - \lambda_e)/\lambda_e$; where λ_o is the observed wavelength and λ_e is the emitted wavelength. A derivation of Equation 1.2 is given in Appendix A. A subroutine for calculating K–corrections is presented in Richardson 2001 [75].

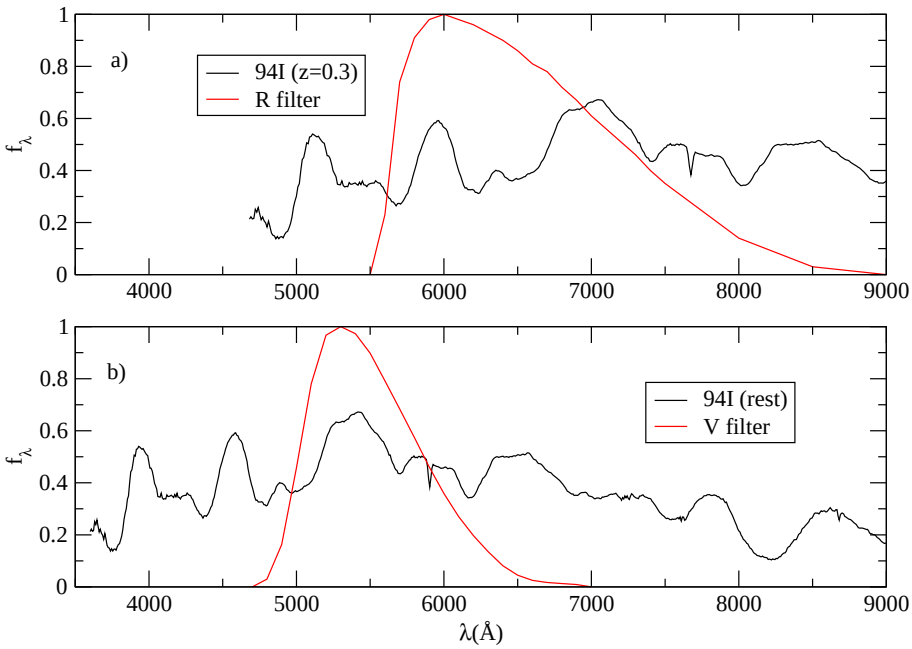

Figure 1.5: a) A spectrum redshifted to z=0.3 with the R filter function. b) That same spectrum in the SN's rest frame with the V filter function.

Chapter 2

The SUSPECT Supernova Data Archive

2.1 Introduction

In the past, supernova (SN) spectra were only available from the observers who take them. For those astronomers who aren't observers, but use SN spectra in their research, it was often difficult to obtain spectra. There has been a real need for a database of SN spectra to be available to everyone. The same can be said for SN photometry. Photometry, however, is mostly available in the literature; but it would be nice to have as much data as possible collected and available from one place, in electronic form.

This is the motivation behind the SUSPECT supernova data archive [1]. SUSPECT is an online database for the uniform collection, storage and dissemination of SN spectra and photometry. The spectra are stored in FITS format not only because FITS is a standard format, but also because the FITS header contains important information about a given spectrum. Most of the spectra we collect from observers are already in FITS format. Sometimes the spectra are

[1] http://www.nhn.ou.edu/~suspect

only available in ASCII and we convert them to FITS. To increase the number of spectra in the database we are dependent on observers to provide them. Because photometry is taken directly from the literature, increasing the number of light curves simply means we need to spend the time collecting and recording the data. We have collected data on 115 SNe. We have spectra for 106 of these SNe and photometry for 20. We haven't been working on the photometry as long as the spectra, but the light curve numbers are increasing at a steady rate.

It should also be mentioned that SUSPECT can be very useful for education. A free and ready source of spectral data such as this can be used to help astronomy students learn about spectral features; what ions are responsible for the features and what the shape of a feature says about the SN that produced the spectrum. SUSPECT would also be useful for students who are beginning to do research.

Most of the spectra and light curves used in later chapters are available from the SUSPECT database. A look at the database from the user's point of view is given in §2.2. We present a more detailed look at the inner workings of the database in §2.3.

2.2 The User's Perspective

A flowchart of the database, as seen from the user's perspective, is shown in Figure 2.1. The user has the choice of several pages to go to from the homepage (Figure 2.2): SEARCH, SN INDEX, CONTRIBUTE, CREDITS, EMAIL, OUTLINE OF THE DATABASE or BULK DOWNLOADS. The best place to start is probably the OUTLINE page. This page quickly explains the basic com-

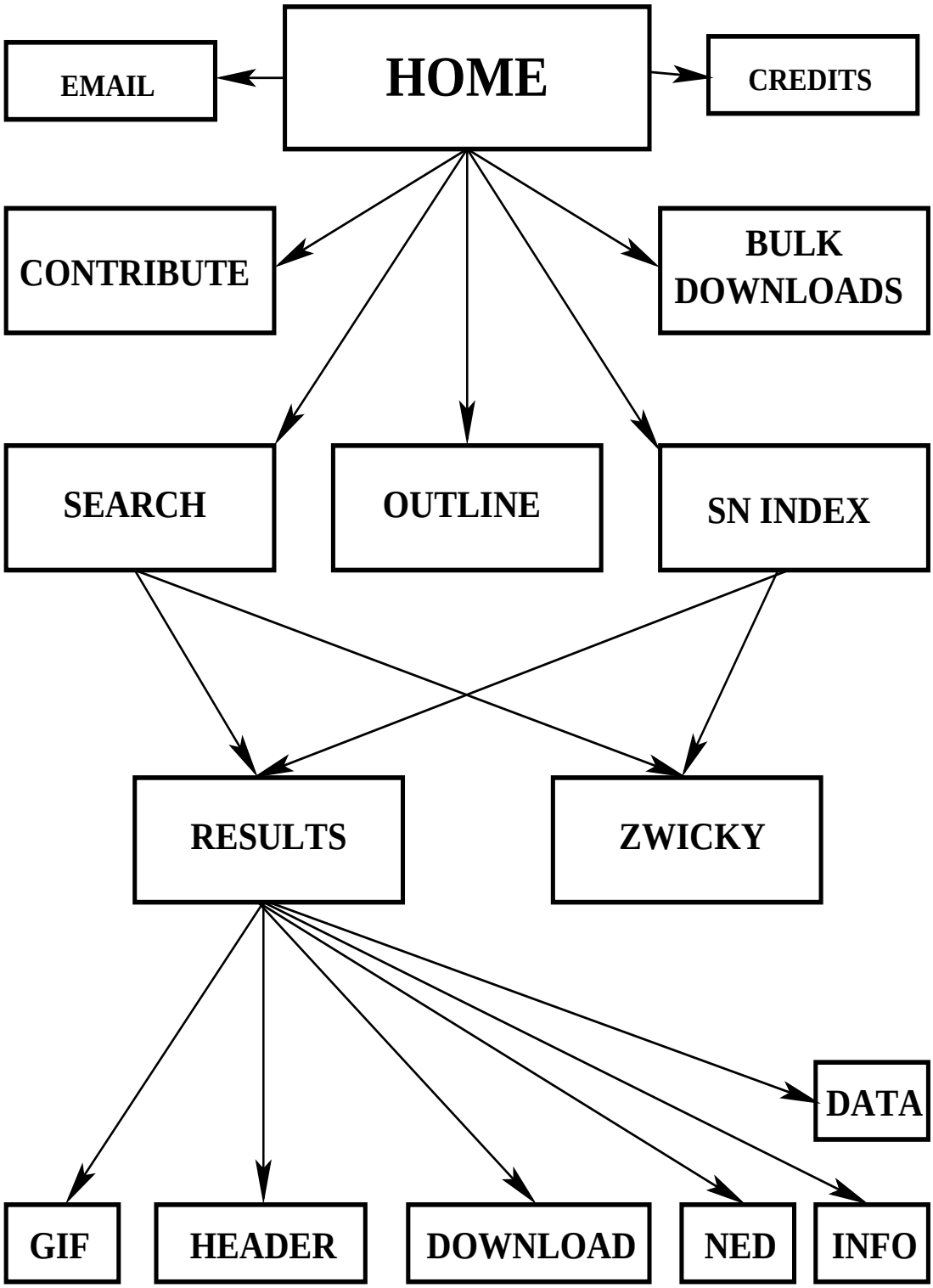

Figure 2.1: Flowchart of SUSPECT for the user.

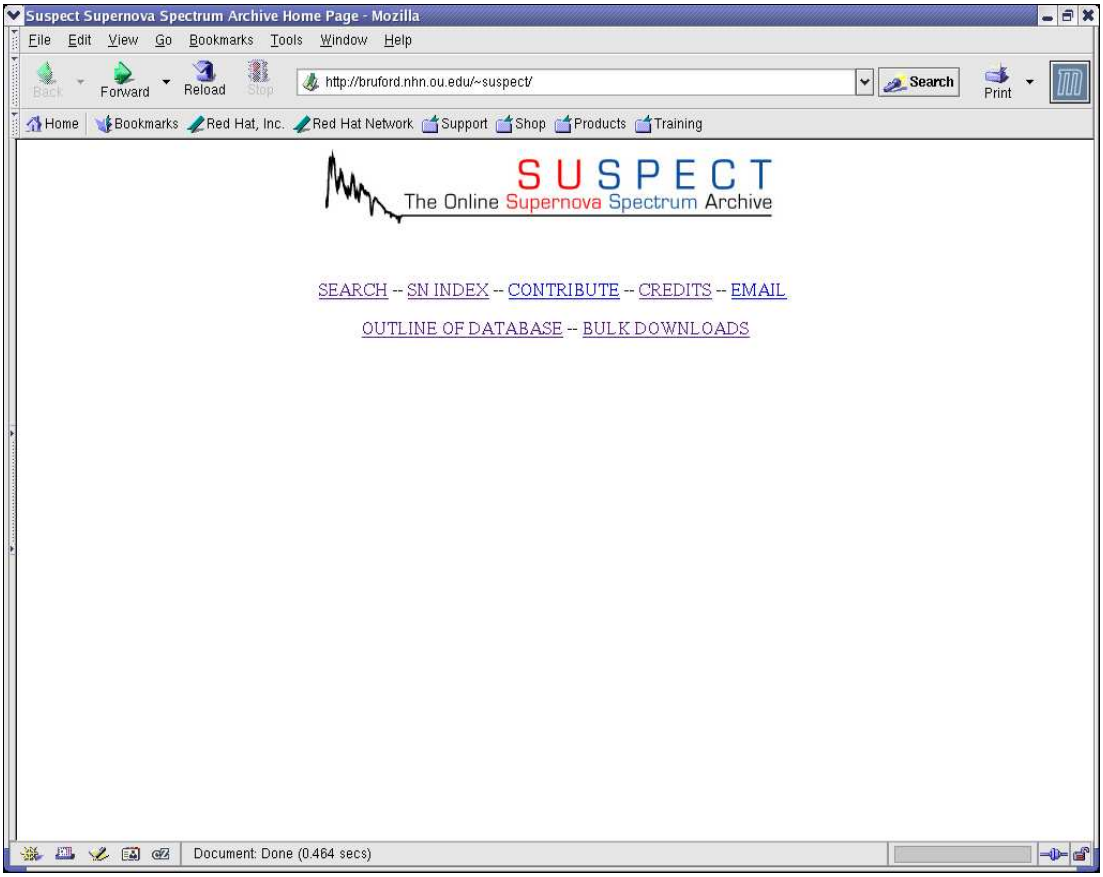

Figure 2.2: The HOME page.

ponents of the site. To retrieve data, the user would go to either the SEARCH page (Figure 2.3) or the SN INDEX page (Figure 2.4). If the user needs help understanding any of the search fields on the SEARCH page the fields are set up with hypertext that, if clicked on, will take them to a more detailed explanation of that field. The user can search by SN name, SN type or date range (Gregorian or Julian). Spectra can also be searched for by phase (days since maximum light) or wavelength range. Light curves can be searched for by band–pass.

Sometimes it is more convenient to simply look at a list of the supernovae (SNe) in the database. This can be done on the SN INDEX page. The type of the SN is given next to the name. There are also three columns after the SN

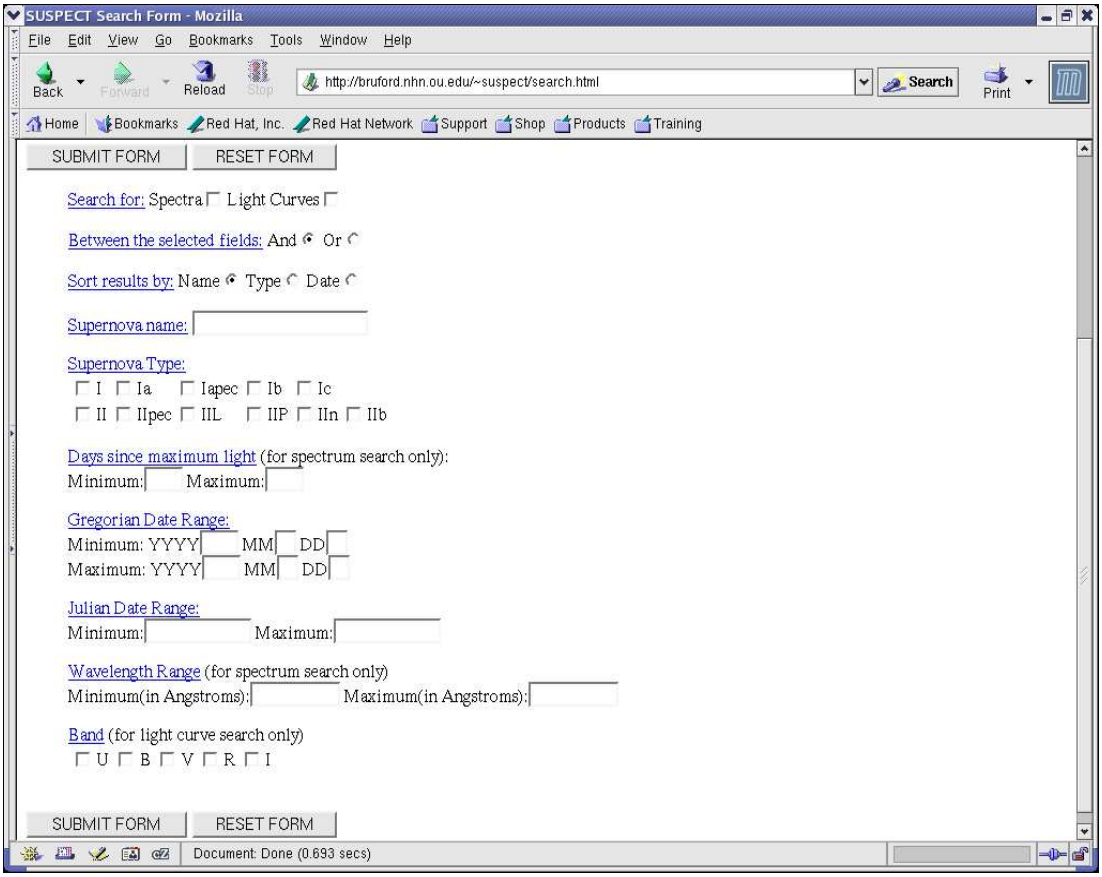

Figure 2.3: The SEARCH page.

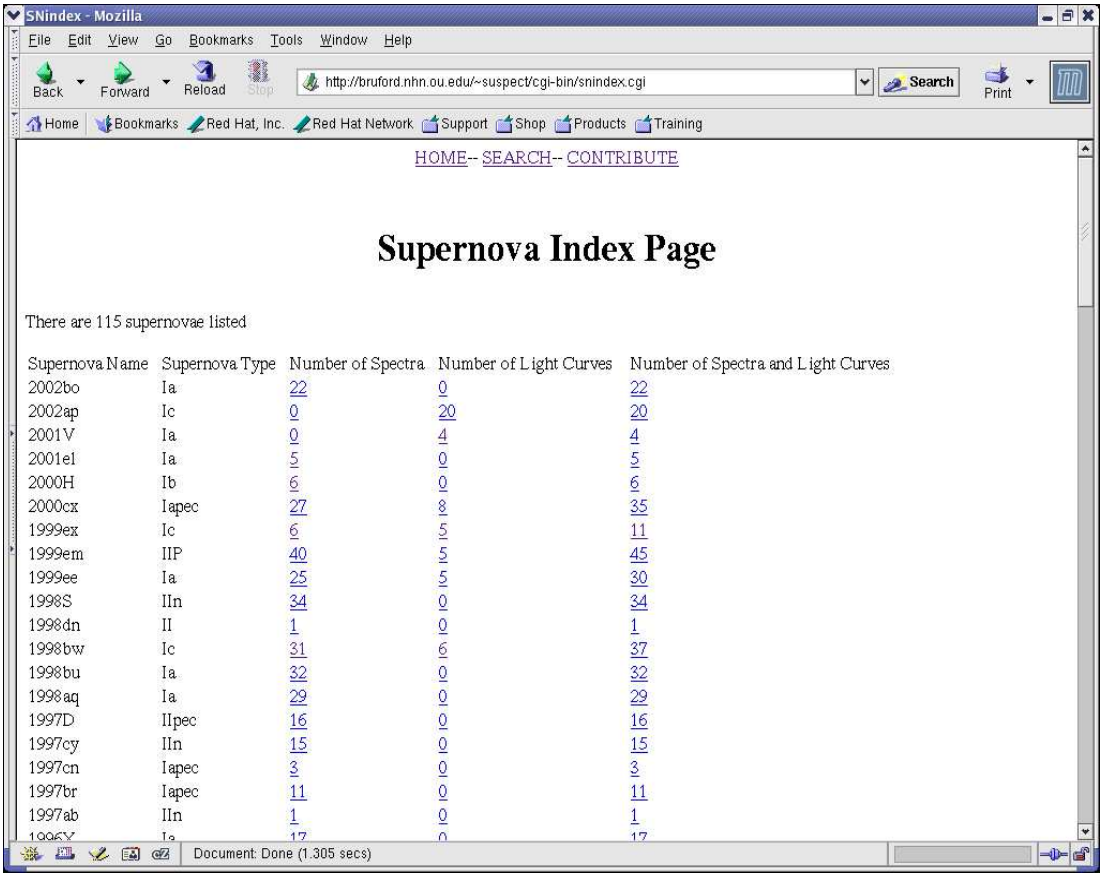

Figure 2.4: The SN INDEX page.

type column. One gives, in hypertext, the number of spectra for that SN. The next gives, in hypertext, the number of light curves for that SN, and the third gives, also in hypertext, the total number of both spectra and light curves. From the hypertext, a search will be carried out as if it were done from the SEARCH page, returning all of the spectra, light curves or both for that SN.

After a search is initiated the user is taken to either the RESULTS page or the ZWICKY page. The ZWICKY page is where the user is informed that the search produced no results. The search parameters are also given there for reference. On the RESULTS page (Figure 2.5) some basic information is given for each of the data sets found (whether spectra or light curves). Each data set is listed separately with the SN name and type shown in hypertext which, if clicked on, will run the search again for all of the data for either that SN or that type.

For spectra, there are several choices. The user can download the FITS file, view/download the ASCII data, pull up a plot of the spectrum, view the FITS header, go to the NED (NASA/IPAC Extragalactic Database) site for that SN or go to in General Information page. The General Information page (Figure 2.6) gives basic information on the SN and its host galaxy. It also gives some basic information on the spectrum and provides a link to the ADS (The NASA Astrophysics Data System) page for the reference paper.

For light curves, the choices on the RESULTS page are similar to that for spectra. The user can view/download the photometry data in ASCII format where the dates are given in either Gregorian data (GD) or Julian date (JD). A plot of the light curve can be pulled up. As with the spectra, there is link a

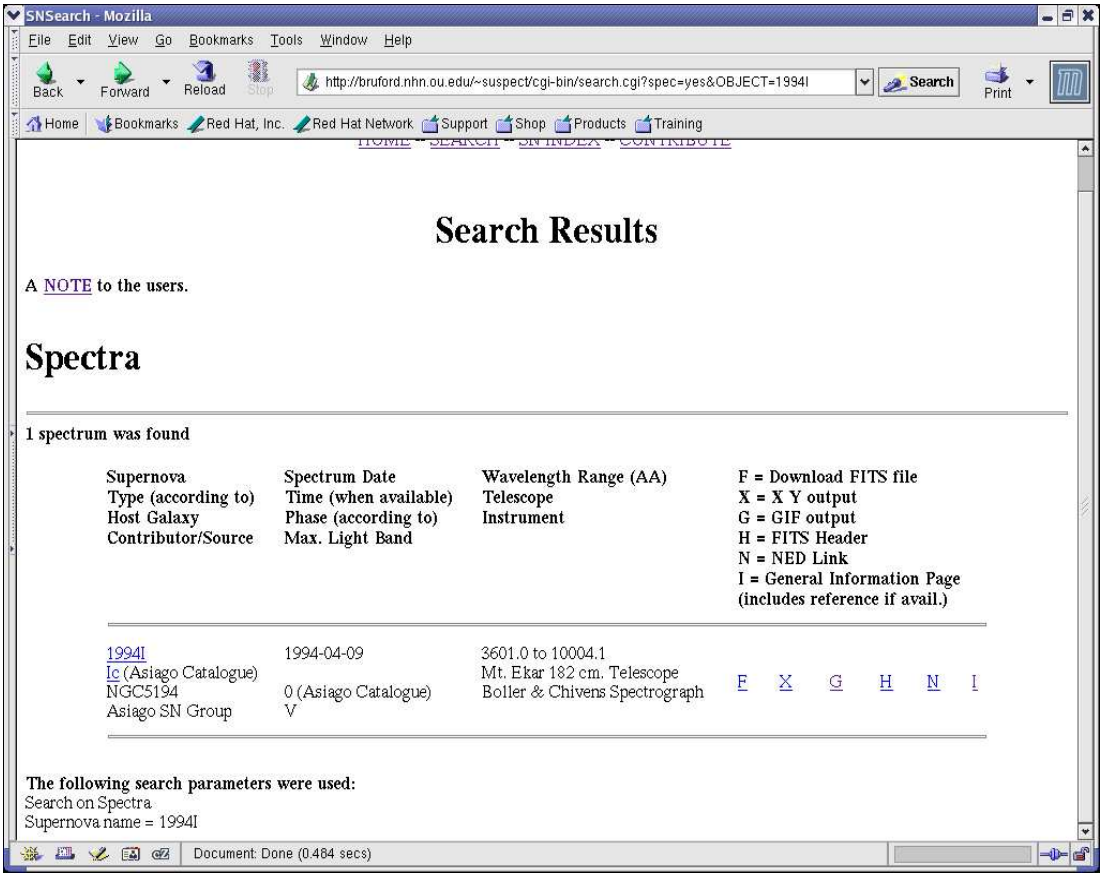

Figure 2.5: The RESULTS page.

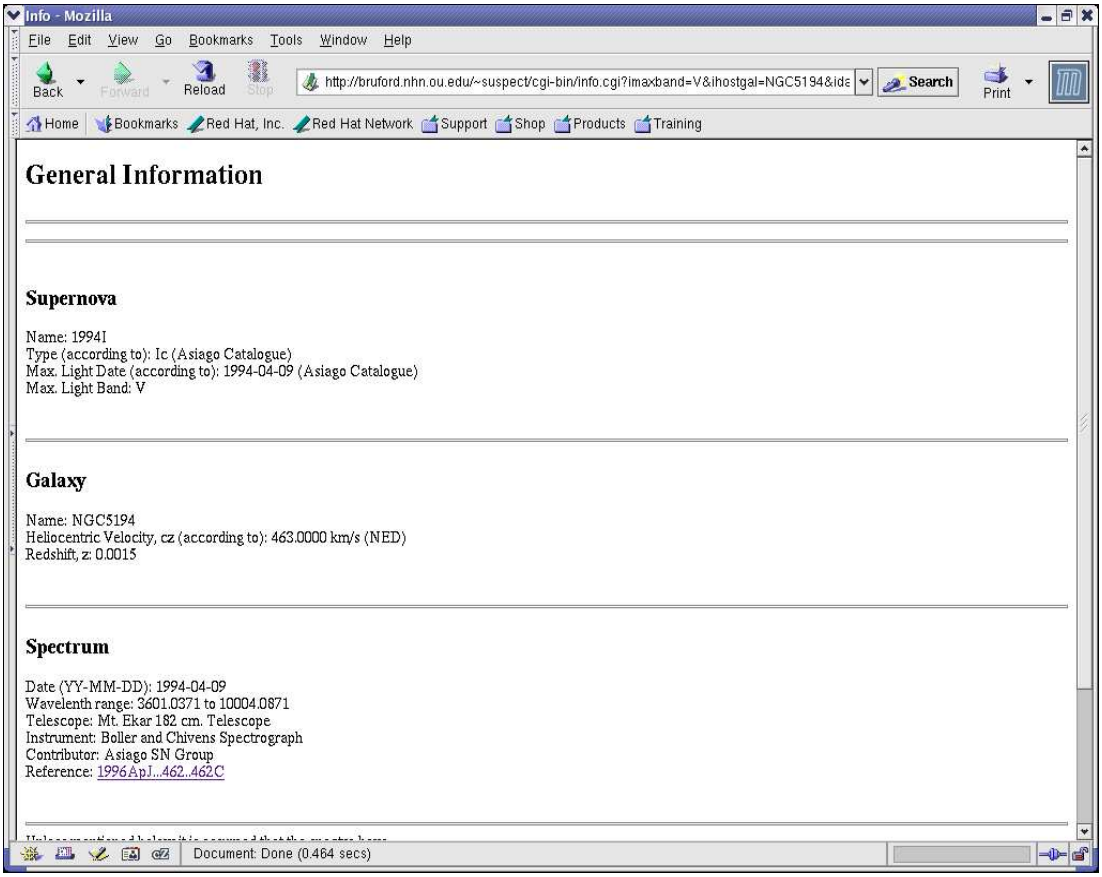

Figure 2.6: The General Information page.

to NED for the SN and a General Information page for the photometry data. Besides giving basic information on the SN and its host galaxy, the General Information page also lists every magnitude value (with GD and JD) in the light curve along with any other specific information available for each point (i.e. uncertainty, telescope, instrument and general comments). There is also an ADS link to the reference paper.

2.3 Behind The Scenes

For the structure of the database we use the open source "Structured Query Language", MySQL. With this, a relational database can be designed so that fairly complex searches may be carried out. DBI (DataBase Interface) is used as the interface between MySQL and the Perl scripts which we have written. CGI (Common Gateway Interface) is used as the interface between the Perl scripts and the Apache web server. HTML is the interface between Apache and the user. A flowchart of the basic operations of the SUSPECT database is shown in Figure 2.7.

The actual database and the FITS files are stored on the the computer's hard drive and are accessed by MySQL and Perl scripts, respectively.

For the SEARCH page we use an HTML form generated by the file search.html. From here a Perl script, search.cgi, is called. This is the longest and most complicated script written for SUSPECT. The search parameters sent to this script from search.html are first rewritten into two long strings that MYSQL will understand. One string is the search string (containing the search parameters) and the other is the sort string (for sorting the results). These strings are then sent

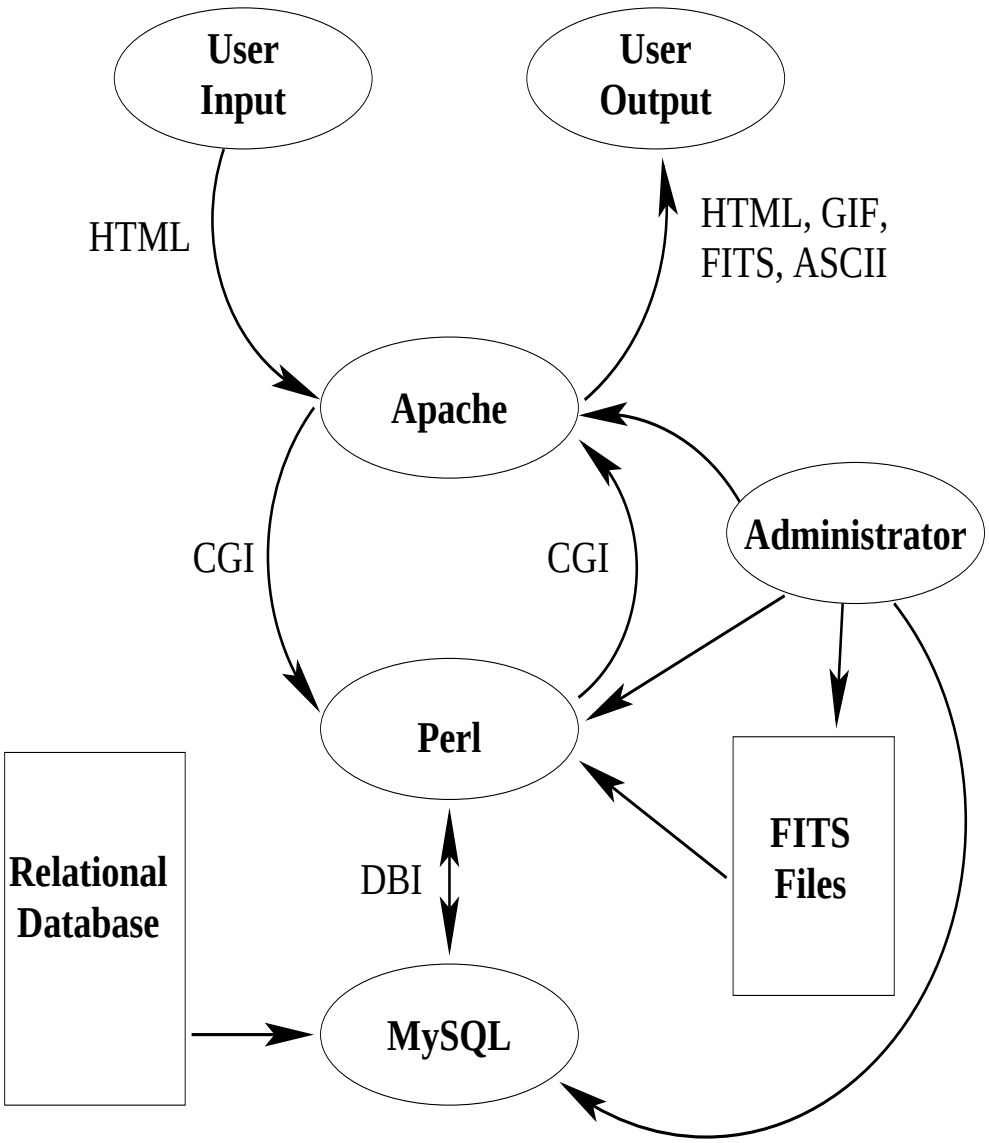

Figure 2.7: Flowchart of the basic operations of SUSPECT.

to the Perl module spectra.pm, which queries the database through MySQL.

In spectra.pm there are several subroutines. The first one, new, is used to add some conditions to the search string that are necessary to the search and then execute a query to the database. From the results, it builds a hash of lists for the autoloader. A hash is similar to a one-dimensional array, except instead of using integers for keys it uses character strings. This hash is then read back into search.cgi where the data can be retrieved from the hash using the subroutine AUTOLOAD. The data are then displayed on the RESULTS page by search.cgi.

From the RESULTS page a number of other scripts can be called. The SN name or SN type hypertext (href) can initiate other searches. For spectra, there is a script, fits2fits, that can be called that will retrieve the FITS data from the FITS file where it is stored. Another script, fits2xy, will retrieve and then convert the FITS data to ASCII and display it. For light curves, a script, db2xy.cgi, can be called to retrieve the photometry points and display them with either GD or JD. For the conversion between GD and JD, subroutines in a Perl module, jdate.pm, are used. There are scripts (fits2gif for spectra and db2gif.cgi for photometry) that will retrieve the data and display it in a GIF plot using PGPLOT. One script, fits2head, will retrieve only the header from the FITS file of a spectrum and display that. There is a hypertext (href) that will connect the user to the NED page for the particular supernova of that data set. Finally, scripts (info.cgi for spectra and db2xy.cgi for photometry) can be called for displaying additional information about a particular data set on the General Information page.

Chapter 3

Absolute–Magnitude Distributions of Stripped–Envelope Supernovae

3.1 Introduction

In a recent paper (Richardson et al. 2002 [76], hereafter R02) we carried out a comparative study of the absolute magnitudes of all supernovae (SNe) in the Asiago Catalog. Because of the large number of SNe in the sample, we did not attempt to estimate the extinction of each SN in its host galaxy, and we did not assign uncertainties to individual SN absolute magnitudes. In this paper we look more closely at the absolute–magnitude distributions of stripped–envelope supernovae (SE SNe), by assigning uncertainties to each of the quantities that enter into the absolute–magnitude determination, including host galaxy extinction. By SE SNe we mean SNe of Types IIb, Ib and Ic. (The subset containing only SNe Ib and Ic are referred to as SNe Ibc.) The progenitors of SE SNe are stars that have lost most or all of their hydrogen envelope. This can happen by strong winds (such as in Wolf Rayet stars) or through mass transfer to a companion star (such as in Roche–Lobe Overflow or even a common–envelope

phase). The light curves of SE SNe are powered by the radioactive decay of ^{56}Ni, so the absolute magnitudes are closely related to the ejected ^{56}Ni masses, and in turn to the stellar progenitors and explosion mechanisms. Since the discovery of the apparent association of GRB980425 with SN 1998bw (Galama et al. 1999 [32]), and more importantly the confirmation by spectra of a SN associated with GRB030329 [34], SE SNe have become important in better understanding GRBs. The absolute–magnitude distributions of SE SNe are important in understanding the events responsible for GRBs.

The data for this study are described in §3.2, the analysis of the absolute–magnitude distributions is presented in §3.3, and comments on the spectra of the events of this sample are offered in §3.4. The results are summarized briefly in §3.5.

3.2 Data

R02 worked with the B band, but for SE SNe the V band happens to be the one for which most data are available. In order to calculate the peak visual absolute magnitude for each SN we collected data on the peak apparent visual magnitude, the distance, the foreground Galactic extinction, and the host galaxy extinction, all with assigned uncertainties. We were able to find data for 3 SNe IIb (Table 3.1), 10 SNe Ib (Table 3.2) and 13 SNe Ic (Table 3.3), a significant improvement on the 18 SNe Ibc to which R02 could assign absolute magnitudes (SNe IIb were not considered).

SN	*Galaxy*	*V*	μ
1987K	NGC4651	14.4 ± 0.3(1)	31.09 ± 0.03[a](2)
1993J	NGC3031	10.86 ± 0.02(4)	27.80 ± 0.08[a](5)
1996cb	NGC4651	13.90 ± 0.03(7)	31.09 ± 0.03[a](2)

Table 3.1a: Data for SNe IIb

SN	A_V*(Galactic)*	A_V*(host)*	M_V
1987K	0.088 ± 0.014	0.2 ± 0.2(3)	-17.0 ± 0.4
1993J	0.266 ± 0.043	0.36 ± 0.22(6)	-17.57 ± 0.24
1996cb	0.100 ± 0.016	0.10 ± 0.10(7)	-17.39 ± 0.11

Table 3.1b: Data for SNe IIb, continued
[a]Cepheid calibrated distance
[b] Nearby Galaxies Catalog (Tully 1988 [89])
[c] Luminosity Distance (H_0=60,Ω_M=0.3, Ω_Λ=0.7; references are for redshifts)
References – (1) Filippenko et al. (1988) [27], (2) Average of Cepheid distances for NGC4321, NGC4535, NGC4548 and NGC4639 in the same group; Freedman et al. (2001) [30], (3) Filippenko (1987) [26], (4) van Driel et al. (1993) [91], (5) Freedman et al. (2001) [30], (6) Richmond et al. (1994) [77], (7) Qiu et al. (1999) [73]

SN	*Galaxy*	*V*	μ
1954A	NGC4214	9.3 ± 0.2(1,2)	27.13 ± 0.23(3)
1983N	NGC5236	11.3 ± 0.2(7)	27.49 ± 0.14[a](6)
1984I	E323–G99	15.98 ± 0.20(8)	33.66 ± 0.20[c](9)
1984L	NGC 991	13.8 ± 0.2(11)	31.85 ± 0.20[b]
1991D	LEDA84044	16.4 ± 0.3(14)	36.67 ± 0.05[c](15)
1998dt	NGC 945	17.42 ± 0.5(16)	34.45 ± 0.14[c](17)
1999di	NGC 776	17.91 ± 0.8(16)	34.60 ± 0.13[c](18)
1999dn	NGC7714	16.48 ± 0.3(16)	33.37 ± 0.23[c](18)
1999ex	IC5179	16.63 ± 0.04(20)	33.80 ± 0.19[c](9)
2000H	IC 454	17.30 ± 0.03(22)	34.11 ± 0.16[c](9)

Table 3.2a: Data for SNe Ib

SN	A_V*(Galactic)*	A_V*(host)*	M_V
1954A	0.072 ± 0.012	0.05 ± 0.05(4)	-17.95 ± 0.31
1983N	0.228 ± 0.037	0.37 ± 0.37(7)	-16.79 ± 0.44
1984I	0.344 ± 0.055	0.05 ± 0.05(10)	-18.07 ± 0.29
1984L	0.091 ± 0.015	0.23 ± 0.23(11)	-18.37 ± 0.36
1991D	0.205 ± 0.033	0.05 ± 0.05(14)	-20.52 ± 0.31
1998dt	0.085 ± 0.014	0.35 ± 0.35(4)	-17.46 ± 0.63
1999di	0.322 ± 0.052	0.67 ± 0.67(4)	-17.68 ± 1.05
1999dn	0.174 ± 0.028	0.05 ± 0.05(19)	-17.11 ± 0.38
1999ex	0.067 ± 0.011	1.39 ± 1.00(21)	-18.63 ± 1.02
2000H	0.760 ± 0.122	0.60 ± 0.60(4,23)	-18.17 ± 0.63

Table 3.2b: Data for SNe Ib, continued
[a]Cepheid calibrated distance
[b] Nearby Galaxies Catalog (Tully 1988 [89])
[c] Luminosity Distance (H_0=60,Ω_M=0.3, Ω_Λ=0.7; references are for redshifts)
References – (1) Schaefer (1996) [81], (2) Leibundgut et al. (1991) [51] and references therein, (3) Drozdovsky et al. (2002) [24], (4) Calculated from the NaI D line, (6) Same group as NGC5253; Freedman et al. (2001) [30], (7) Clocchiatti et al. (1996a) [18], (8) Estimated from Leibundgut et al. (1990) [50], (9) NED, (10) Phillips & Graham (1984) [68], (11) Wheeler & Levrealt (1985) [95], (12) Estimated from Tsvetkov (1986) [87], (13) Same group as NGC4258; Freedman et al. (2001) [30], (14) Benetti et al. (2002) [9] and references therein, (15) Maza & Ruiz (1989) [57], (16) Estimated from Matheson et al. (2001) [56], (17) Jha et al. (1998) [42], (18) Asiago SN Catalog; Barbon et al. (1999) [6], (http://web.pd.astro.it/∼supern/), (19) Ayani et al (1999) [4], (20) Stritzinger et al. (2002) [85], (21) Hamuy et al. (2002) [36], (22) Krisciunas & Rest (2000) [48], (23) Benetti et al. (2000) [8]

SN	*Galaxy*	*V*	μ
1962L	NGC1073	13.13 ± 0.10(1)	31.39 ± 0.20[b]
1964L	NGC3938	13.6 ± 0.3(3)	31.72 ± 0.14[a](4)
1983I	NGC4051	13.6 ± 0.3(5)	31.72 ± 0.14[a](4)
1983V	NGC1365	13.80 ± 0.20(6)	31.27 ± 0.05[a](7)
1987M	NGC2715	14.7 ± 0.3(8)	32.03 ± 0.23[b]
1990B	NGC4568	15.75 ± 0.20(10)	30.92 ± 0.05[a](7)
1991N	NGC3310	13.9 ± 0.3(11,26)	31.84 ± 0.20[b]
1992ar	ANON	19.54 ± 0.34(13)	39.52 ± 0.01[c](14)
1994I	NGC5194	12.91 ± 0.02(16)	29.62 ± 0.15(17)
1997ef	UGC 4107	16.47 ± 0.10(19)	33.90 ± 0.18[c](20)
1998bw	E184–G82	13.5 ± 0.3(21)	33.13 ± 0.26[c](20)
1999cq	UGC11268	16.1 ± 0.6(23)	35.64 ± 0.08[c](20)
2002ap	NGC 628	12.37 ± 0.04(24)	30.41 ± 0.20[b]

Table 3.3a: Data for SNe Ic

SN	A_V *(Galactic)*	A_V *(host)*	M_V
1962L	0.130 ± 0.021	$0.80 \pm 0.80(2)$	-19.19 ± 0.83
1964L	0.071 ± 0.011	$0.56 \pm 0.56(2)$	-18.75 ± 0.65
1983I	0.043 ± 0.007	$0.93 \pm 0.31(5)$	-19.09 ± 0.45
1983V	0.068 ± 0.011	$0.56 \pm 0.22(6)$	-18.10 ± 0.30
1987M	0.085 ± 0.014	$1.4 \pm 0.6(9)$	-18.82 ± 0.71
1990B	0.108 ± 0.017	$2.63 \pm 1.00(10)$	-17.91 ± 1.02
1991N	0.075 ± 0.012	$1.0 \pm 1.0(12)$	-19.02 ± 1.06
1992ar	0.048 ± 0.008	$0.25 \pm 0.25(15)$	-20.28 ± 0.42
1994I	0.115 ± 0.018	$1.4 \pm 0.5(18)$	-18.22 ± 0.52
1997ef	0.141 ± 0.022	$0.05 \pm 0.05(19)$	-17.62 ± 0.21
1998bw	0.194 ± 0.031	$0.05 \pm 0.05(22)$	-19.87 ± 0.40
1999cq	0.180 ± 0.029	$0.39 \pm 0.39(23)$	-20.11 ± 0.72
2002ap	0.161 ± 0.026	$0.03 \pm 0.03(25)$	-18.23 ± 0.21

Table 3.3b: Data for SNe Ic, continued
[a] Cepheid calibrated distance
[b] Nearby Galaxies Catalog (Tully 1988 [89])
[c] Luminosity Distance (H_0=60, Ω_M=0.3, Ω_Λ=0.7; references are for redshifts)
References – (1) Schaefer (1995) [80], (2) Estimated from Porter & Filippenko (1987) [70], (3) Leibundgut et al. (1991) [51] and references therein, (4) Same group as NGC3982; Saha et al. (2001) [79], (5) Tsvetkov (1985) [86], (6) Clocchiatti et al. (1997) [20], (7) Freedman et al. (2001) [30], (8) Filippenko et al. (1990) [28], (9) Nomoto et al. (1990) [64], (10) Clocchiatti et al. (2001) [22], (11) Tsvetkov (1994) [88], (12) Grothues & Schmidt–Kaler (1991) [35], (13) Clocchiatti et al. (2000) [21], (14) Phillips & Hamuy (1992) [69], (15) Estimated from Clocchiatti et al. (2000) [21], (16) Richmond et al. (1996) [78], (17) Feldmeier et al. (1997) [25] (18) Barth et al. (1996) [7], (19) Estimated from Iwamoto et al. (2000) [40], (20) NED, (21) Monard (1998) [62], (22) Nakamura et al. (2001) [63], (23) Estimated from Matheson et al. (2000) [55], (24) Gal–Yam et al. (2002) [33] (data actually taken from the website http://wise-obs.tau.ac.il/∼avishay/local/2002ap/index.html), (25) Klose et al. (2002) [45], (26) Korth (1991a) [46]

3.2.1 Peak Apparent Magnitudes

For most SNe the apparent magnitude and its uncertainty were taken directly from the literature, but in some cases these values were not given so it was necessary for us to estimate them. For SNe 1998dt, 1999di and 1999dn we used an uncalibrated R band light curve (Matheson et al. 2001 [56]) together with a calibrated spectrum to determine the peak V magnitude. We used the spectrum

that was nearest to maximum light to calculate the R magnitude at that epoch, and used the R light curve to determine the R magnitude at peak. Then we calculated the $V - R$ color from the spectrum to determine V at peak. We examined the available data on $V - R$ versus time for SNe Ibc and estimated the total uncertainty in V accordingly. A similar method was used for SN 1999cq (Matheson et al. 2000 [55]). The peak apparent magnitude for SN 1992ar was taken from Clocchiatti et al. (2000) [21] who, from the limited data available, presented two possible light curves, with different peak magnitudes; we adopted the average. In Tables 3.1 – 3.3 we can see that the peak V magnitudes are the dominant uncertainties in six cases: the SN IIb 1987K, the SNe Ib 1991D, 1998dt and 1999di, and the SNe Ic 1992ar and 1999cq.

3.2.2 Distances

Distance moduli were, for the most part, obtained as in R02. When possible we used a Cepheid calibrated distance to the host galaxy or a galaxy in the same group as the host galaxy. The second choice was the distance given in the Nearby Galaxies Catalog (NGC, Tully 1988 [89]), rescaled from $H_0 = 75$ km s^{-1} Mpc^{-1} used in the NGC to our choice of $H_0 = 60$. We adopted an uncertainty of 0.2 magnitudes in the distance modulus (combined in quadrature with the uncertainty resulting from the radial velocity uncertainty of the host galaxy). One significant change is that a new distance, based on the tip of the red giant branch, has become available for NGC 4214, the host of SN 1954A (Drozdovsky et al. 2002 [24]). We adopt this distance in preference to assigning the (longer) NGC distance as in R02. Now SN 1954A no longer appears to be

an overluminous SN Ib. Another exception is the distance we used for SN 1994I. This distance was taken from Feldmeier, Ciardullo, & Jacoby (1997) [25] who used the Planetary Nebula Luminosity Function Method. They showed that distances determined from this method are consistent with distances determined from Cepheids. The third choice was the luminosity distance (Kantowski, Kao, & Thomas 2000 [43]) calculated for the redshift of the host galaxy (in each of these cases $cz > 2000$ km s^{-1}) and assuming $H_0 = 60$, $\Omega_M = 0.3$ and $\Omega_\Lambda = 0.7$. A different choice of H_0 would rescale the absolute magnitudes and different choices of Ω_M and Ω_Λ would have very small effects on this sample. The uncertainty in the luminosity distance was calculated assuming a peculiar velocity of 300 km s^{-1}. For many of the events of our sample the uncertainty in the distance modulus is significant, although it is never dominant.

3.2.3 Extinction

The Galactic extinction is from Schlegel, Finkbeiner, & Davis (1998) [82]. Values were taken from NED[1] and converted from A_B to A_V. In all cases the uncertainties in the Galactic extinction are comparatively small.

When possible the host galaxy extinction and its uncertainty were taken directly from the literature. When only the equivalent width of the interstellar NaI D line, $W(D)$, in the host was available we calculated $E(B-V)$ from the relation $E(B-V) = 0.16W(D)$ (Turatto, Benetti, & Cappellaro 2002 [90]) and then used $A_V = 3.1E(B-V)$. In this case we took the uncertainty to be as large as the extinction, up to a maximum uncertainty of 1.0 magnitude.

[1]The NASA/IPAC Extragalactic Database (NED) is operated by the Jet Propulsion Laboratory, California Institute of Technology, under contract with the National Aeronautics and Space Administration.

The host galaxy extinction for SN 1983V was taken from Clocchiatti et al. (1997) [20]. Porter & Filippenko (1987) [70] reported that the HII region associated with SN 1983V was not as prominent as the one associated with SN 1962L but about the same as the one associated with SN 1964L. Having only this information to go on we assigned the A_V(host) value of SN 1983V to SN 1964L. For SN 1962L we took the average value of all other SNe Ic in our sample (which is larger than the extinction of SN 1983V). For SNe 1962L and 1964L we assigned an uncertainty as large as the extinction.

For SN 1990B we took the host galaxy extinction from Clocchaitti et al. (2001) [22]. They quoted two values, one determined from the NaI D line and one from the color excess; we chose to use the latter. They did not quote an uncertainty except to say that it was large and unknown, so we assigned a large uncertainty of 1.0 magnitude.

Grothues & Schmidt–Kaler (1991) [35] give the extinction for various regions of NGC 3310, the host galaxy of SN 1991N. Near the position of SN 1991N (Barth et al. 1996 [7]) the visual extinction was 1 to 2 magnitudes with an uncertainty of about 1 magnitude. Because the SN was most likely inside rather than behind the HII region this extinction is probably an overestimate. We adopted $A_V = 1.0 \pm 1.0$.

SE SNe tend to be associated with star formation, therefore they tend to be significantly extinguished in their host galaxies. Tables 3.1 – 3.3 show that for many events in our sample the uncertainty in the host galaxy extinction is the dominant uncertainty, and overall it is the largest source of uncertainty for our sample.

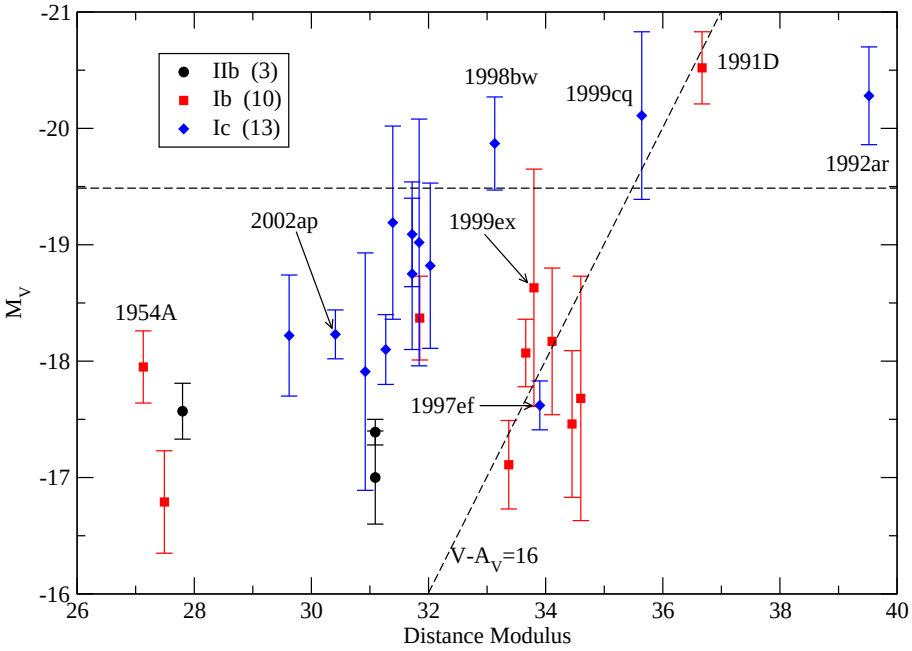

Figure 3.1: Absolute visual magnitude versus distance modulus with the vertical error bars shown. Some key SNe are labeled.

3.3 Analysis

Absolute visual magnitude is plotted against distance modulus in Fig. 3.1. The slanted dashed line is the line of constant apparent visual magnitude (less the total extinction) of 16. The horizontal dashed line is the SN Ia "ridge line" at $M_V = -19.5$, shown here for comparison. The tendency of intrinsically brighter SNe to be at larger distances, and the fact that all but a few of the SNe are to the left of the slanted line, are obvious consequences of the strong observational bias in favor of the discovery and follow–up of brighter SNe. The absence of SNe in the lower right part of the figure is a selection effect against lower–luminosity events at large distance, and the absence of SNe in the upper left is due to the fact that overluminous events are uncommon, so none happen to have been seen in relatively nearby galaxies. Considering that the events of this sample

have been discovered in so many different ways, we make no attempt to correct the absolute magnitude distribution for bias. Instead, we emphasize that in this study we are simply characterizing the available observational sample of SE SNe; a sample in which overluminous events are strongly over–represented relative to less luminous ones.

R02 considered the possibility that SNe Ibc can be divided into two luminosity groups: normal SNe Ibc that are less luminous than SNe Ia, and overluminous SNe Ibc that are more luminous than SNe Ia. We consider that possibility here also. As can be seen in Fig. 3.1, four events of our sample, three SNe Ic and one SN Ib, are above the SN Ia ridge line.

The mean absolute magnitude and its standard deviation, both weighted and unweighted, for the whole sample as well as for several subsets of the sample, are given in Table 3.4. The weighted mean of the whole sample is $M_V = -17.96 \pm 0.06$, with $\sigma = 0.90$. When SE SNe are separated into normal and bright we have $M_V = -17.72 \pm 0.07, \sigma = 0.50$ for the normals and $M_V = -20.26 \pm 0.20, \sigma = 0.31$ for the brights. Comparing the normal SNe Ib and Ic, the unweighted means differ by 0.69 magnitudes in the sense that SNe Ic are brighter than SNe Ib, but the weighted means differ by only 0.34 magnitudes so a difference between normal SNe Ib and Ic is not firmly established by these data.

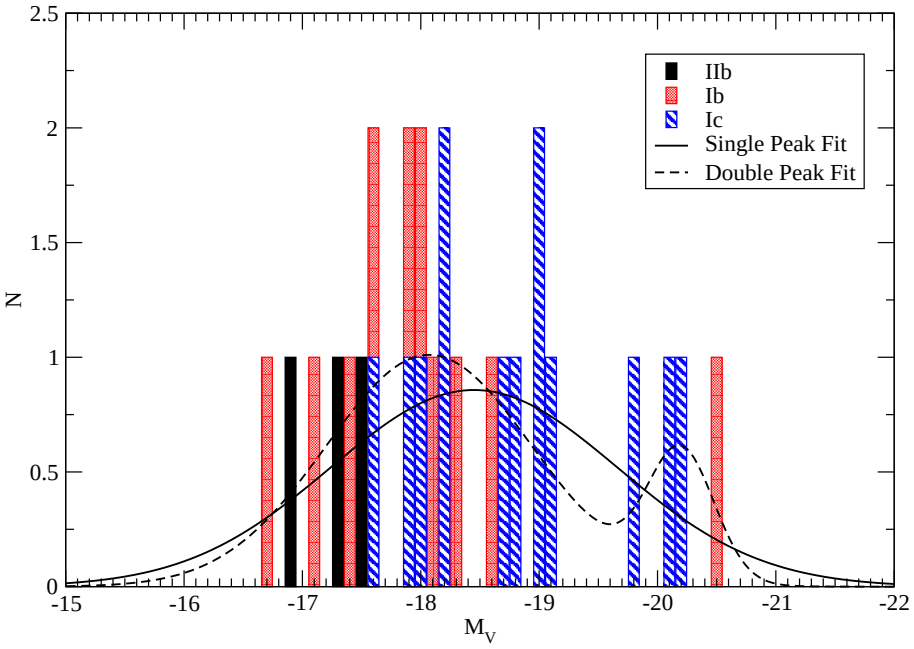

Figure 3.2: A histogram of SE SN absolute magnitudes, with 0.1 magnitude bin width. The best single Gaussian and double–Gaussian fits (see text) are also shown.

	Weighted		Unweighted		
Data Set	$\overline{M}_V$	σ	$\overline{M}_V$	σ	N
All SE	-17.96 ± 0.06	0.90	-18.38 ± 0.20	1.01	26
Bright SE	-20.26 ± 0.20	0.31	-20.20 ± 0.14	0.27	4
Normal SE	-17.72 ± 0.07	0.50	-18.05 ± 0.15	0.69	22
IIb only	-17.40 ± 0.10	0.15	-17.32 ± 0.17	0.29	3
Ib only	-18.28 ± 0.13	1.20	-18.07 ± 0.33	1.03	10
Ic only	-18.45 ± 0.11	0.86	-18.86 ± 0.24	0.85	13
Normal Ib	-17.80 ± 0.14	0.56	-17.80 ± 0.20	0.60	9
Bright Ic	-20.07 ± 0.27	0.23	-20.09 ± 0.12	0.21	3
Normal Ic	-18.14 ± 0.12	0.48	-18.49 ± 0.17	0.55	10

Table 3.4: Mean and Standard Deviation for Various Data Sets.

A histogram of the absolute magnitudes is shown in Fig. 3.2. (Note that in this figure the bright SNe are to the right, which is the reverse of the figures in R02). Fig. 3.2 also shows the best Gaussian fit to all of the data, determined by the χ^2 test using the mean absolute magnitude and dispersion as parameters. The results were $\overline{M}_V = -18.45$ and $\sigma = 1.21$, but the low probability of 28%

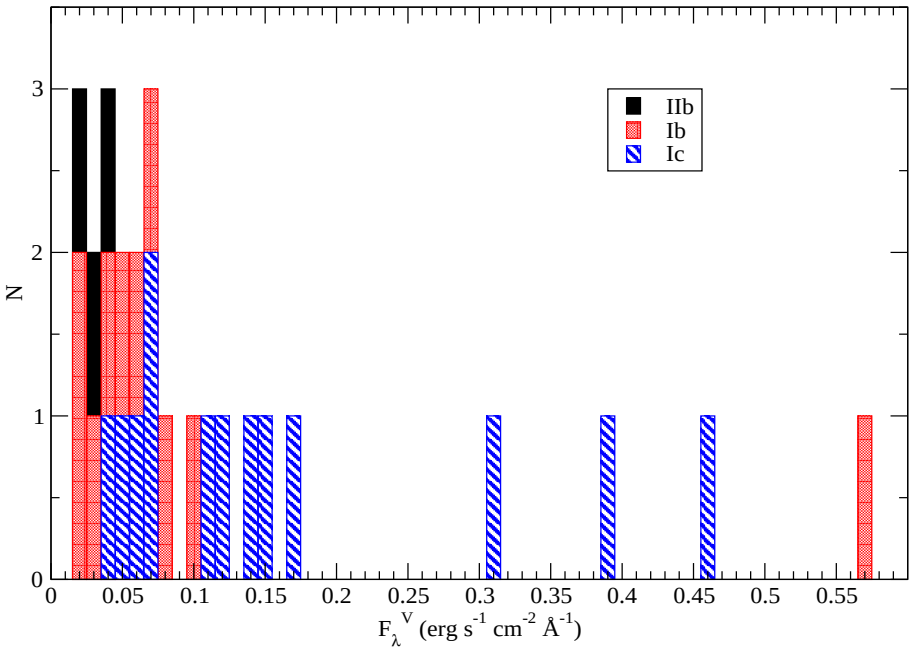

Figure 3.3: A histogram of absolute visual flux in bins of 0.01 erg s^{-1} cm^{-2} $Å^{-1}$.

confirms what is apparent to the eye: the distribution is not adequately fit by a Gaussian.

Considering the possibility of two luminosity groups we also fit the data to a double–peak distribution. To do this we used the equation:

$$f(x) = f_0\left(w\exp\left[-\frac{(x-x_1)^2}{2\sigma_1^2}\right] + \exp\left[-\frac{(x-x_2)^2}{2\sigma_2^2}\right]\right). \tag{3.1}$$

Here, there are five parameters: x_1 and x_2 (the two mean absolute magnitudes), σ_1 and σ_2 (the two dispersions) and the weighting factor, w. The normalization factor, f_0, is equal to $(1+w)^{-1}$. The results for the double–peak distribution are: $\overline{M}_{V,1} = -20.20$, $\overline{M}_{V,2} = -18.07$, $\sigma_1 = 0.28$, $\sigma_2 = 0.87$ and $w = 0.18$. The probability of this fit is 45%; a little better but still quite low.

Fig. 3.3 shows a histogram of fluxes, instead of absolute magnitudes. Here the visual flux is what one would measure at a distance of 10 pc from the SN.

In terms of flux the bright events appear more separated from the rest, and the flux distribution obviously can not be fit by a Gaussian.

3.4 Comments on Spectra

Here we comment briefly on the spectroscopic characteristics of the events of our present sample.

3.4.1 Type IIb

The spectra of SNe IIb have an interesting evolution. At early times they resemble the spectra of SNe II with strong Hα and Hβ P–Cygni features. At late times they resemble the spectra of SNe Ib where the Balmer lines have been replaced with HeII lines. There are three SNe IIb in this study; SNe 1987K, 1993J and 1996cb.

At early times (around peak brightness) the Hα feature of SNe IIb will begin to narrow and the emission peak will begin to flatten. The Hα peak flattens as the HeII λ6678 line begins to form. This indicates the thinning of the hydrogen layer and the emergence of the helium layer of the ejecta. The balmer lines in SN 1996cb are stronger and more similar to SN 1987A, with the exception of the flattened emission peak, than to SN 1993J at early times (Qiu et al. 1999 [73]). This could be an indication that SN 1996cb had a thicker hydrogen layer than SN 1993J.

While there are some differences, the spectra of SNe IIb are quite similar. There don't appear to be any SNe IIb which can be considered spectroscopically peculiar.

3.4.2 Type Ib

Branch et al. (2002) [14] studied the optical spectra of a dozen SNe Ib selected on the basis of having deep HeI absorption features. The events of their sample displayed a rather high degree of spectral homogeneity, except that three also contained deep Hα absorptions. Of the 11 SNe Ib in the present sample, seven were in the sample of Branch (2003) [15]: SNe 1983N, 1984L, 1998dt, 1999dn, 1954A, 1999di, and 2000H, with the last three being the "deep–Hα" events of Branch et al. (2002) [14]. We find that all seven of these events have absolute magnitudes within the normal SN Ib range, and we see no significant difference between the absolute magnitudes of the deep–Hα events and the others.

The single available spectrum (Leibundgut, Phillips, & Graham 1990 [50]) of one of the SNe Ib in our present sample, SN 1984I, covers a limited wavelength range so that little can be said except that it does appear to be a SN Ib.

SN 1991D has been discussed by Benetti et al. (2002) [9] and Branch (2003) [15]. Its spectra were different from those of the Branch et al. (2002) [14] sample: the HeI absorptions were less deep and the velocity at the photosphere near the time of maximum light was lower. Thus the single overluminous SN Ib of our sample also had an unusual spectrum.

SN 1999ex was observed by Hamuy et al. (2002) [36] who referred to it as an intermediate Type Ib/c because of its relatively weak HeI lines. Branch (2003) [15] refers to it as a "shallow helium" SN Ib because its HeI lines were clearly present, although weaker than in the events of the Branch et al. (2002) [14] sample. While this event had an unusual spectrum, according to Table 3.2 it had a normal luminosity.

To summarize SNe Ib: the single overluminous SN Ib of our sample had an unusual spectrum, but not all events that had unusual spectra were overluminous.

3.4.3 Type Ic

The spectra of SNe Ic exhibit considerable diversity (Matheson et al., 2001 [56]); but five events of our sample, SNe 1983I, 1983V, 1987M, 1990B, and 1994I can be said to have had typical SN Ic spectra. The limited available spectra of three others, SNe 1962L, 1964L, and 1991N, also show no indication of peculiarity. The luminosities of all eight of these events are consistent with normal.

As is well known, SN 1998bw, associated with GRB 980425 (Galama et al. 1999 [32]), was an overluminous SN Ic, and the unusually broad spectral features of SN 1998bw indicated a very high kinetic energy of the ejected matter (Patat et al. 2001 [67]). Two other SNe Ic of our sample, SNe 1997ef (Mazzali, Iwamoto, & Nomoto 2000 [58]) and 2002ap (Kinugasa et al. 2002 [44]), also had broad spectral features, although not as broad as those of SN 1998bw; these two SNe Ic were *not* overluminous.

Apart from SN 1998bw, the other two overluminous SNe Ic of our sample are SNe 1992ar and 1999cq. Clocchiatti et al. (2000) [21] conclude that the one available spectrum of SN 1992ar is (with the exception of a weaker CaII H&K absorption feature) remarkably similar to a spectrum of the Type Ic SN 1983V, which as mentioned above had normal spectra. Matheson et al. (2000) [55] interpret the one good spectrum of SN 1999cq as that of a SN Ic but with unusual (so far unique) narrow lines of HeI superimposed. The spectrum of

SN 1999cq certainly is unusual.

SN 1999as is probably the brightest SN Ic known, with an absolute magnitude brighter than -21.4 (Hatano et al. 2001 [38]). However, there is no peak apparent magnitude available, therefore it is not included in our present sample. Its spectrum was quite unusual.

For SNe Ic: two of the three overluminous events (three of four, counting SN 1999as) are known to have had unusual spectra. Not all events having normal luminosities have typical SN Ic spectra: as mentioned above, SNe 1997ef and 2002ap had unusually broad lines.

3.5 Summary

We have used the available data to characterize the absolute magnitude distributions of the SE SNe in the current observational sample. It is clear that most SE SNe have a "normal" luminosity, which at $M_V = -17.96 \pm 0.06$ is more than a magnitude dimmer than SNe Ia. One sixth of the current sample of SE SNe are overluminous, i.e., more luminous than SNe Ia, but these are strongly favored by observational selection so the true fraction of SE SNe that are overluminous is much lower than one sixth. The small size of the sample and the considerable absolute magnitude uncertainties, especially those due to host galaxy extinction, still prevent an absolute magnitude difference between SNe Ib and Ic from being firmly established. Three of the four (or four of five, with SN 1999as) overluminous SE SNe are known to have had unusual spectra, but a few of the normal luminosity SE SNe also had unusual spectra. Much more data on SE SNe are needed in order to better determine the absolute mag-

nitude distributions, and to correlate absolute magnitudes with spectroscopic characteristics.

Chapter 4

Light Curves of Stripped–Envelope Supernovae

4.1 Introduction

Going beyond the peak absolute–magnitude distributions, we now look at the absolute light curves (LCs) of SE SNe. V–band data were collected for two SNe IIb, seven SNe Ib and 11 SNe Ic. Of the SNe Ic, three are considered to be hypernovae. The observational sample of LCs presented here show a great deal of variation; not only in peak brightness, but also in the width of the peak and the slope of the late–time tail. In order to relate the shape and overall brightness of the LCs to more physical quantities we fit the data to a LC model.

The observational data collected are described in §4.2. The model used and the fits to the observed data are discussed in §4.3. The results are presented in §4.4 and a brief summary is given in §4.5.

4.2 Data

Observational LC data in the V band were found for most, but not all, of the SNe in Chapter 3. For a few of the SNe, only R band or unfiltered LC data

were available. The LC data for many of the SNe were available from the same reference as the peak magnitude. Often it was necessary to collect data from a number of sources in order to get as much coverage as possible. For SN1962L, only the photoelectric observations from Bertola (1964) [10] were used. For SN1994I, most of the data were taken from Richmond et al. (1996) [78], but all of this data was within about 65 days of peak. In order to include some late–time points in the LC two points were added from Clocchiatti et al. (1997) [20]. A complete list of the SNe that have V–band LCs and their references are given in Table 4.1.

SN Name	*SN Type*	*Reference*	*SN Name*	*SN Type*	*Reference*
1993J	IIb	[5],[91],[52]	1962L	Ic	[10]
1996cb	IIb	[73]	1983I	Ic	[86]
1954A	Ib	[51],[81],[93]	1983V	Ic	[20]
1983N	Ib	[18]	1987M	Ic	[28]
1984I	Ib	[50]	1990B	Ic	[22]
1984L	Ib	[37],[83],[95]	1991N	Ic	[46],[47],[88]
1991D	Ib	[9]	1992ar	Ic	[21]
1999ex	Ib	[85]	1994I	Ic	[20], [78]
2000H	Ib	[48]	1997ef	Ic	[40]
			1998bw	Ic	[13],[31],[49], [61],[74]
			2002ap	Ic	[29],[65],[97]

Table 4.1: List of the SNe in the study with LCs, and their references.

The LC data collected for SNe IIb/Ib and Ic are shown in Figures 4.1 and 4.2, respectively. The lines in the figures, connecting the symbols for each SN, are only to help distinguish the data of one SN from the data of another. In the legend of Figure 4.2, the asterisks next to the SN name denotes those SNe Ic that are considered hypernovae. A hypernova is a SE SN with very broad features in its spectra, indicating highly energetic ejecta.

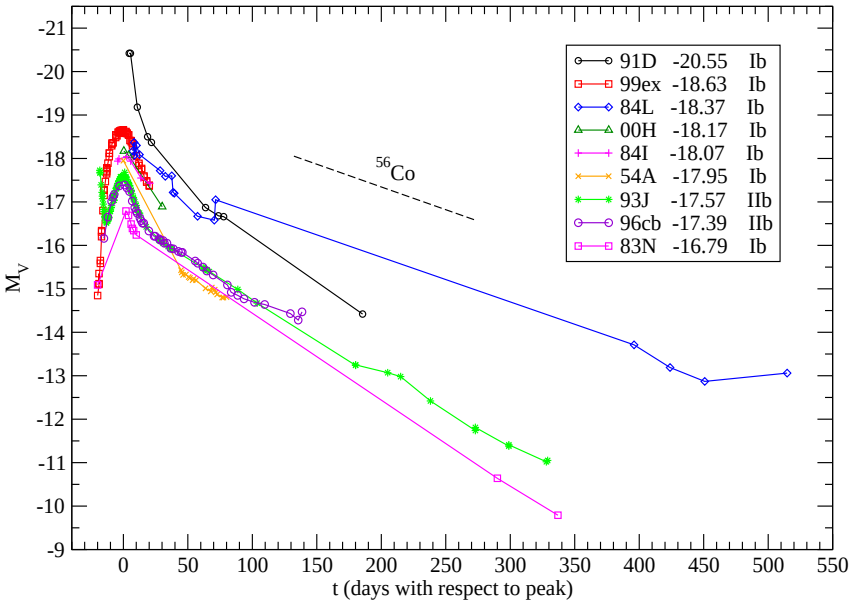

Figure 4.1: The absolute light curves are plotted for SNe IIb and Ib. The peak absolute magnitudes are given in the legend. The ^{56}Co decay slope is shown for reference. Solid lines are only to guide the eye.

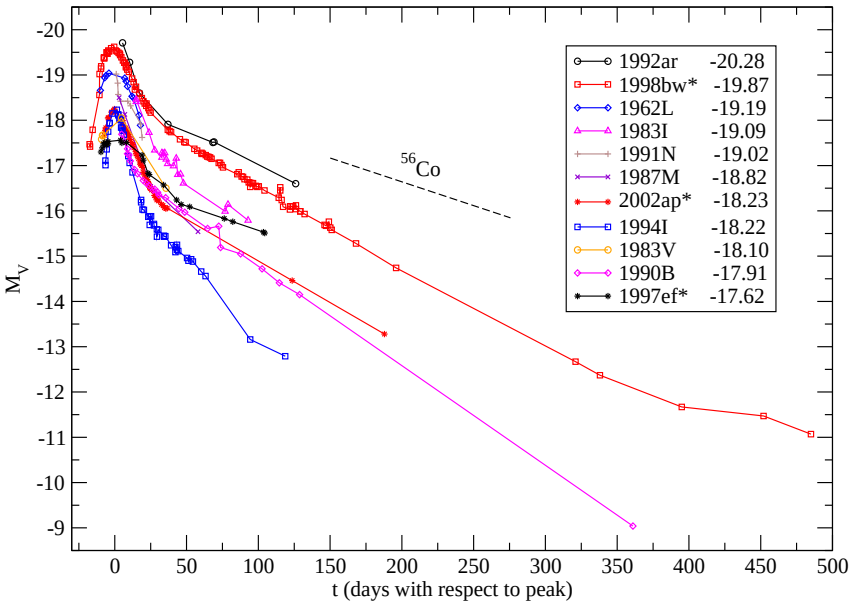

Figure 4.2: The absolute light curves are plotted for SNe Ic. The peak absolute magnitudes are given in the legend. The ^{56}Co decay slope is shown for reference. Solid lines are only to guide the eye. (*=hypernovae)

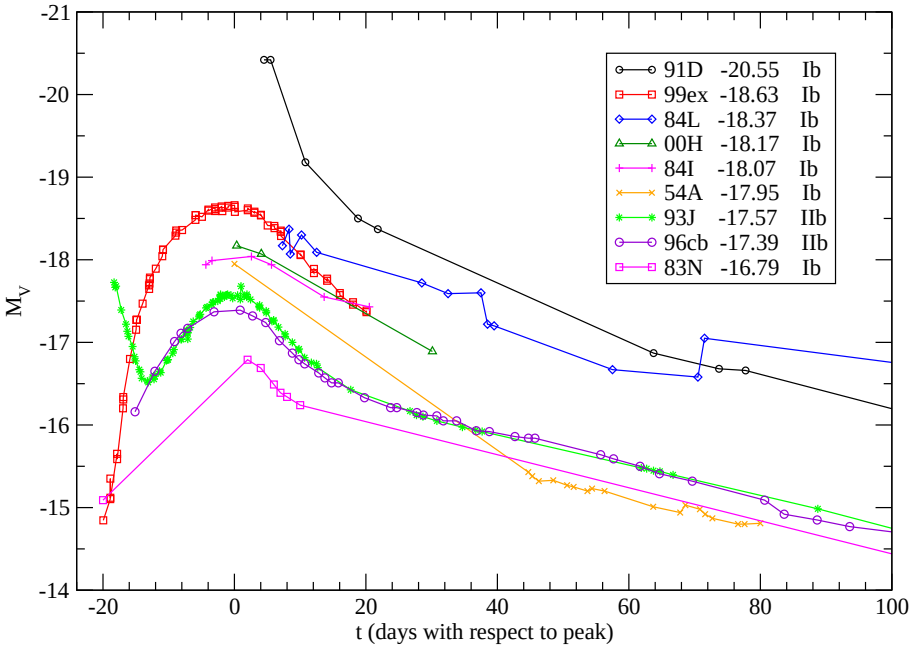

Figure 4.3: Same as Figure 4.1, except shown on a smaller time scale around peak brightness.

The late–time slope of a SN LC is powered, mostly, by the gamma–rays generated in the decay of ^{56}Co. The gamma–rays Compton scatter with free electrons in the ejecta. Subsequently, the very fast moving electrons thermalize in the ejecta emitting optical photons. Some of the gamma–rays escape the ejecta and therefore don't contribute to the tail of the LC. This is why the late–time slopes of the observed data shown in Figures 4.1 and 4.2 are, mostly, faster than the decay slope of ^{56}Co. In Figure 4.1 the slope of SN 1984L is slower than the ^{56}Co decay slope. The early data for SN 1984L appears scattered and likely quite uncertain. On the other hand the late–time data could include galaxy light; it is very difficult to separate the SN light from the galaxy light at late times, when the SN is very dim.

Figures 4.3 and 4.4 are the same as Figures 4.1 and 4.2, respectively, except on a smaller time scale in order to show more detail around the time of peak

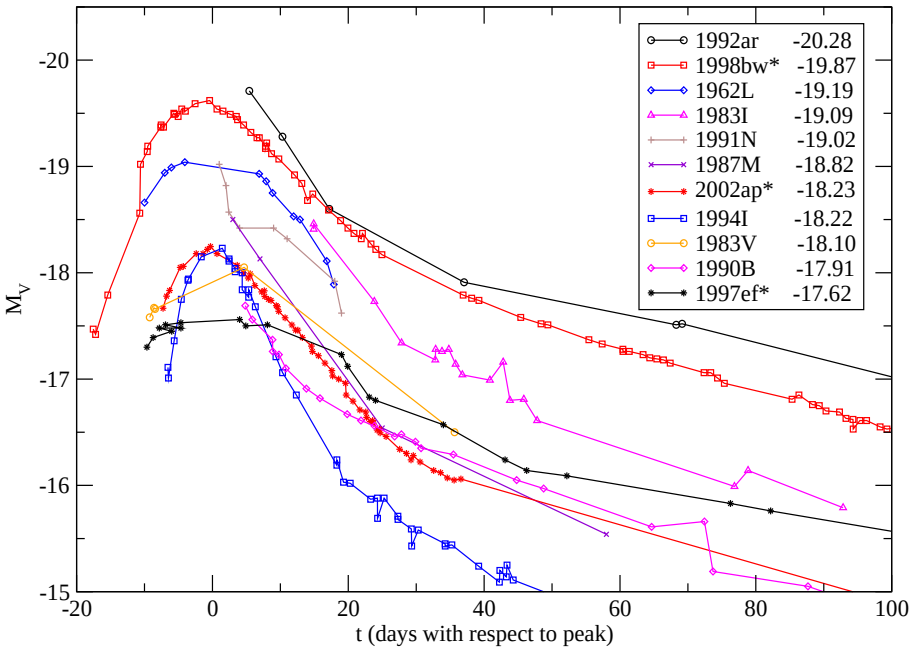

Figure 4.4: Same as Figure 4.2, except shown on a smaller time scale around peak brightness. (*=hypernovae)

brightness. The two SNe IIb LCs shown here are very similar to each other and are quite dim compared to most SNe Ibc. Most notable among the SNe Ib is the extremely bright SN 1991D. It falls off in brightness very fast after peak which hints at a very narrow peak. SN 1994I also has a very fast LC, even though it is usually thought of as a typical SN Ic simply because it was well observed. SN 1983N is the dimmest of the SNe Ib and is also the dimmest SN in the study.

On average, the SNe Ic are brighter than the SNe Ib and IIb. The LCs of SNe Ic also vary over a wide range of peak width. The narrowest peak in the sample appears to be SN 1994I and the widest peak appears to be SN 1997ef.

Model fits for all of the LCs are shown in section 4.4 except for SNe 1954A, 1984I, 1984L and 1991N where the coverage in their visual LCs was too poor for a fit.

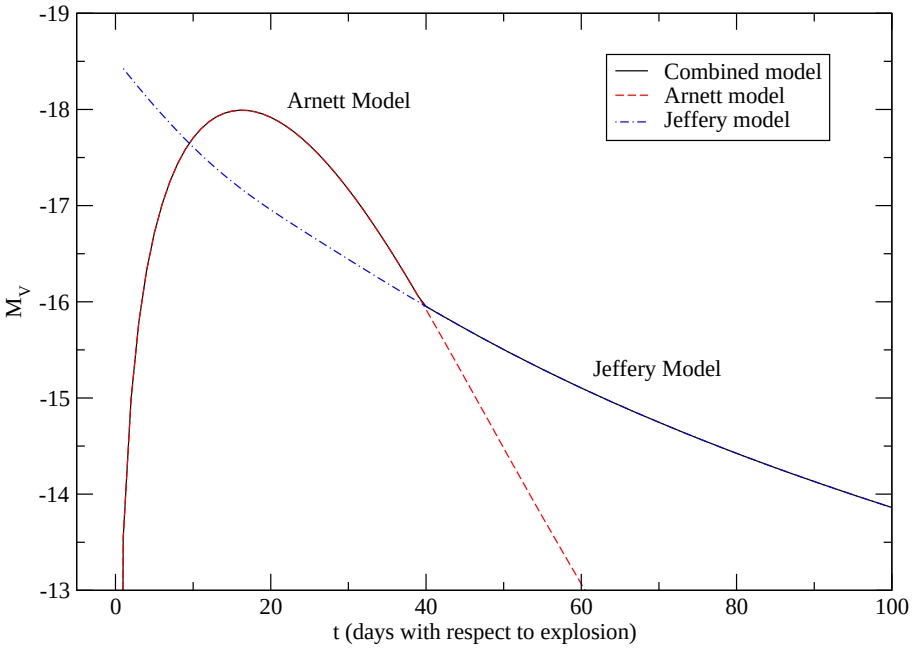

Figure 4.5: Here the combined model is shown by the solid line and the Arnett and Jeffery models are shown as dashed lines.

4.3 The Model

For the peak of the LC, the model of Arnett (1982) [3] was used and for the late–time deposition function the model of Jeffery (1999) [41] was used. The Arnett model results only work at early times, as long as the diffusion approximation remains valid. The Jeffery model is good only at late times when the deposition of gamma–rays dominates the LC. The Arnett model was used until the point after peak brightness when it drops below the Jeffery model (Figure 4.5). At this transition point the change to the Jeffery model is abrupt. This is also the point when the assumptions are the poorest. The general assumptions used here are spherical symmetry with homologous expansion, radiation–pressure dominated at early times, the presence of ^{56}Ni and its concentration toward the center of the ejecta, and finally, optical opacity is constant at early times and gamma–ray

opacity is constant at late times. The equations used for the Arnett part are:

$$L_A(t) = \epsilon_{Ni} M_{Ni} \left(10^{-\frac{\zeta}{2.5}}\right) \left(e^{-x^2}\right) \int_0^x 2ze^{(-2zy+z^2)}dz \tag{4.1}$$

Where, $x \equiv \frac{t}{\tau_m}$ and $y \equiv \frac{\tau_m}{2t_{e,Ni}}$.

$$\tau_m = \sqrt{\frac{\kappa_{opt}}{\beta c}} \sqrt{\frac{6M_{ej}^3}{5E_k}} \tag{4.2}$$

$$\epsilon_{Ni} = \frac{Q_{ph+PE}^{Ni}}{m_{Ni} t_{e,Ni}} \tag{4.3}$$

The equations used for the Jeffery part are:

$$L_J(t) = \epsilon_{Ni} M_{Ni} \left\{ e^{-\frac{t}{t_{e,Ni}}} + G \left(e^{-\frac{t}{t_{e,Co}}} - e^{-\frac{t}{t_{e,Ni}}} \right) \left[f_{PE}^{Co} + f_{ph}^{Co} \left(1 - e^{-(\frac{t_0}{t})^2} \right) \right] \right\} \tag{4.4}$$

$$t_0 = \sqrt{\frac{M_{ej}\kappa_\gamma}{4\pi v_a v_b}} \tag{4.5}$$

$$v_i = v_i^{93J} \sqrt{\frac{\left(\frac{E_k}{M_{ej}}\right)}{\left(\frac{E_k}{M_{ej}}\right)_{93J}}} \tag{4.6}$$

Where $i = a, b$.

$$G = \left(\frac{Q_{ph+PE}^{Co}}{Q_{ph+PE}^{Ni}}\right) \left(\frac{m_{Ni}}{m_{Co}}\right) \left(\frac{t_{e,Ni}}{t_{e,Co} - t_{e,Ni}}\right) = 0.184641 \tag{4.7}$$

The e–folding times for Co and Ni are shown as $t_{e,Co}$ and $t_{e,Ni}$ with values of 111.48 and 8.767 days, respectively. This is the half–life divided by $ln(2)$.

The energy per decay is Q_{ph+PE}; including energy from photons and electron–positron pairs, but not from neutrinos (which escape). The values for Co and Ni are: $Q^{Co}_{ph+PE} = 3.74$ MeV and $Q^{Ni}_{ph+PE} = 1.729$ MeV. The fraction of Q_{ph+PE} from photons is f_{ph} and the fraction from the kinetic energy of electron–positron pairs is f_{PE}. The values for Co are: $f^{Co}_{ph} = 0.968$ and $f^{Co}_{PE} = 3.20 \times 10^{-2}$. The values for the quantities mentioned above are taken from Table 1 of Jeffery (1999) [41]. The mass per nucleus of ^{56}Ni and ^{56}Co are m_{Ni} and m_{Co} (values derived from data at the LBL website: http://ie.lbl.gov/toimass.html). The optical and gamma–ray opacities used are $\kappa_{opt} = 0.4$ and $\kappa_{\gamma} = 0.04$. Arnett (1982) [3] defined β as $4\pi(\alpha I_M/3)$, where $\alpha I_M = 3.290$ (Arnett, 1980 [2]) for uniform density.

The model produces a bolometric LC. Observed bolometric LC data are not often given in the literature, although V–filter LCs (which are more available) are known to have a similar shape. In order to adjust the brightness of the model to better match a V–filter LC a correction (ζ) was used for the early–time part. The value of ζ was determined by calibrating the peak of the LC to that of a typical SN Ia. This was done by fixing E_k to 1 foe (10^{51} erg), M_{ej} to 1.4 $M_{\odot}$ (the Chandrasekhar mass) and M_{Ni} to 0.6 $M_{\odot}$, then adjusting ζ so that the peak magnitude came to -19.5. The value for ζ came to -1.48.

The velocities v_a and v_b are the inner and outer velocities, respectively, within which there is a relatively constant mass density in the ejecta. These values are not known for most of the supernovae in our sample. In Jeffery (1999) [41], these velocities were assigned the values of SN 1987A. A better approximation for SE SNe would be to use the velocities of SN 1993J (the best

observed SE SN) and to rescale these velocities with respect to E_k/M_{ej} for each SN. The SN 1993J velocities used are $v_a = 1000$ km s^{-1} and $v_b = 10,000$ km s^{-1}. The velocities and the E_k/M_{ej} value for SN 1993J were taken from Blinnikov (1998) [12]. The value used for $(E_k/M_{ej})_{93J}$ was 0.51 foe/$M_\odot$.

The model parameters are E_k, M_{ej}, M_{Ni} and t_{shift}. This last parameter shifts the model with respect to time. To find the best χ^2 fit the program was run through a grid of parameter values. The best fit was often very good but had unphysical values for the parameters. To fix this problem the ratio of E_k/M_{ej} was constrained for each SN. Reliable values have been determined from more sophisticated numerical models for about half of the SNe in the sample. A method was developed here to find the E_k/M_{ej} values for the rest of the SNe.

The kinetic energy of a particle is $E_k = \frac{1}{2}Mv^2$. For SN ejecta it is a little more complicated. The mass would have to be M_{ej} and the most reasonable velocity to use would be the photospheric velocity, v_{phot}; which well represents the average velocity of the ejecta. Because we have a system of particles, instead of a single particle, the proportionality constant is not necessarily $\frac{1}{2}$. Actually, it must be a function of time due to the fact that v_{phot} is a function of time and E_k/M_{ej} is constant. For this function we have: $a(t) = (E_k/M_{ej})/v_{phot}^2(t)$.

One common way to determine v_{phot} is to look at the peak of the FeII blend near 5000Å in the SN spectrum. In order to standardize this relation the parameterized SN synthetic–spectrum code SYNOW (Branch et al., 2002 [14]) was used. The relation is shown in Figure 4.6. It was then possible to calculate a(t) for the SNe for which E_k/M_{ej} is known. Figures 4.7 and 4.8 are plots of a(t) for normal SE SNe and hypernovae, respectively, on a log scale. In these

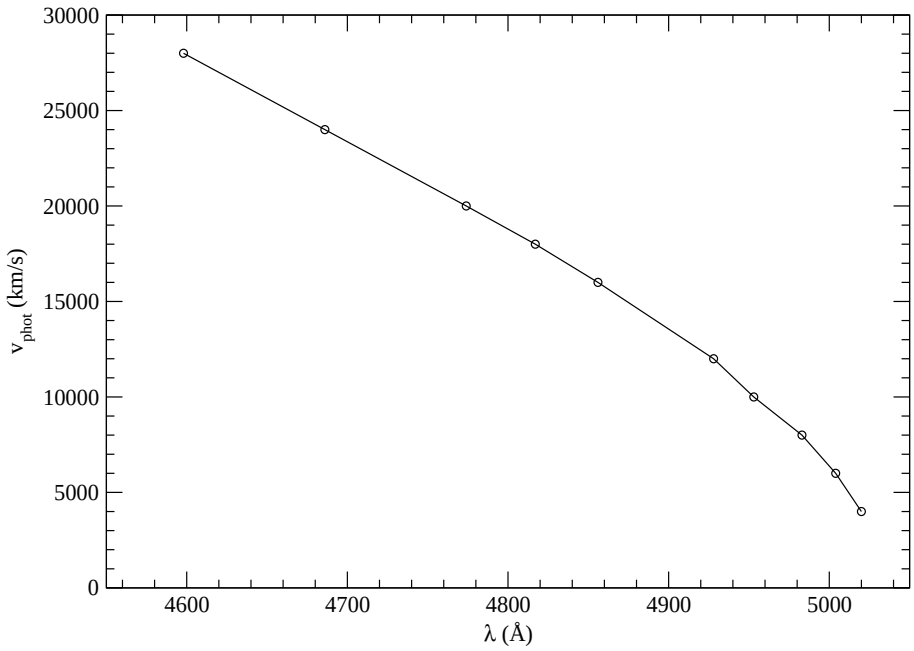

Figure 4.6: The relation between v_{phot} and the peak of the FeII blend near 5000Å are shown as determined by SYNOW.

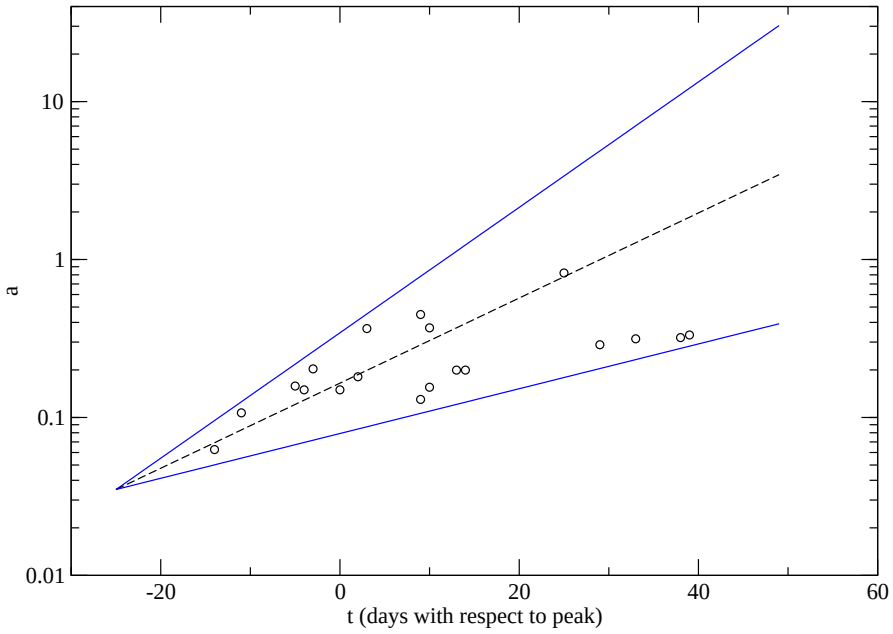

Figure 4.7: For normal SE SNe, a(t) is shown on a log scale with solid lines showing the upper and lower limits and the dashed line showing the mean.

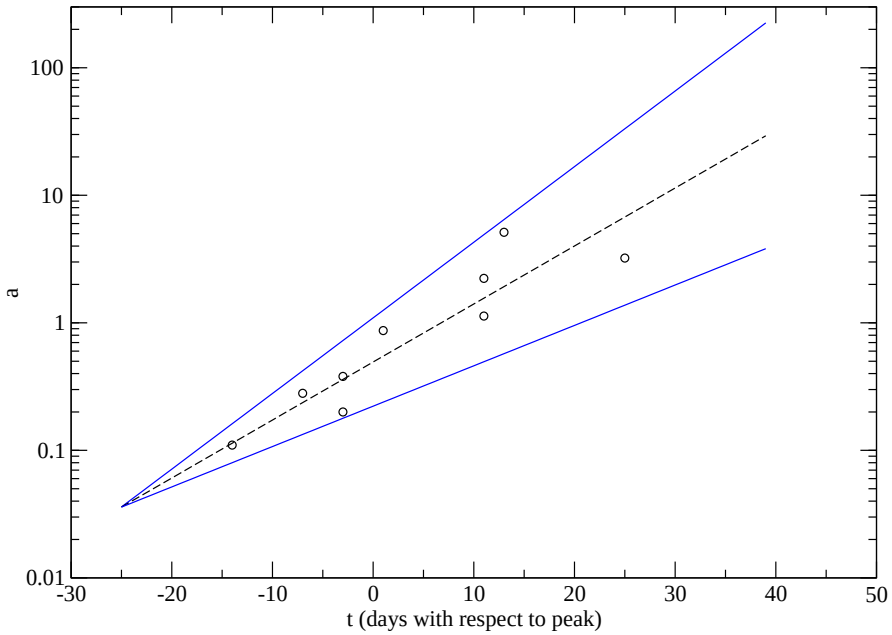

Figure 4.8: For hypernovae, a(t) is shown on a log scale with solid lines showing the upper and lower limits and the dashed line showing the mean.

figures the solid lines are drawn to represent the upper and lower limits for log_{10}(a(t)). The dashed line gives the mean values. The mean values were used for a(t) and the upper and lower limits were used for the uncertainties. It can be seen from these graphs that in order to get a(t), and hence E_k/M_{ej}, with relatively small uncertainties it was necessary to use spectra at early epochs. This makes sense because, as the ejecta expands, the photosphere recedes with respect to the ejecta and v_{phot} becomes less representative of the ejecta. When several early spectra were found for a given SN the weighted average of E_k/M_{ej} was used.

With the remaining three parameters (M_{ej}, M_{Ni} and t_{shift}) the model produced relatively good fits with reasonable parameter values. The amount of ^{56}Ni synthesized in the explosion plays an important role in powering the peak of SE SN LCs. It decays with a half life of 6 days. ^{56}Co is a decay product of

^{56}Ni and, itself, decays with a half life of 77 days to power the tail of the LC. The rise time ($t_{rise} = t_{peak} - t_{explosion}$) is simply taken from the model LC.

4.4 Results

The parameter values determined from the model fits are listed in Table 4.2. Uncertainties were not available for each data point in all LCs. Because of this we used the uncertainty at peak to represent the uncertainty for the entire LC. The uncertainties in M_V given here are different from those listed in Tables 3.1 – 3.3. Each uncertainty here has the uncertainty in E_k/M_{ej} added in quadrature.

SN name	E_k *(foe)*	M_{ej} $(M_\odot)$	M_{Ni} $(M_\odot)$	t_{rise} *(days)*	χ^2_r	δM_V *(mag)*	N
IIb							
1993J	0.66(1)	1.3	0.10	20	2.14	0.26	89
1996cb	0.22(2)	0.9	0.08	20	1.30	0.18	44
Ib							
1983N	0.30(3)	0.8	0.05	18	2.24E−2	0.45	9
1991D	0.25(2)	1.9	$\geq$1.52	27	4.42	0.49	10
1999ex	0.30(2)	0.9	0.25	19	0.967	1.05	71
Ic							
1962L	0.11(2)	0.6	0.37	19	6.92E−3	0.85	11
1983I	0.33(3)	0.7	0.23	17	0.140	0.46	18
1983V	0.99(2)	1.3	0.15	19	3.25E−3	0.35	5
1987M	0.19(4)	0.4	0.13	14	3.49E−3	0.72	4
1990B	0.55(2)	0.9	0.14	18	0.229	1.08	26
1992ar	1.14(2)	1.5	0.84	20	0.103	0.67	7
1994I	0.55(5)	0.5	0.08	14	0.744	0.53	50
1997ef	3.26(6)	3.1	0.16	23	0.491	0.23	22
1998bw	31.0(7)	6.2	0.78	23	2.37	0.41	105
2002ap	2.72(8)	1.7	0.14	19	1.50	0.23	60

Table 4.2: Parameter values from the best χ^2 fit of the model to the data. References for E_k/M_{ej} relation – (1) Blinnikov et al. (1998) [12], (2) E_k/M_{ej} was calculated as described in text, (3) Shigeyama et al. (1990) [84], (4) Nomoto et al. (1990) [64], (5) Young, Baron & Branch (1995) [96], (6) Iwamoto et al. (2000) [40], (7) Nakamura et al. (2001) [63] (8) Mazzali et al. (2002) [59]

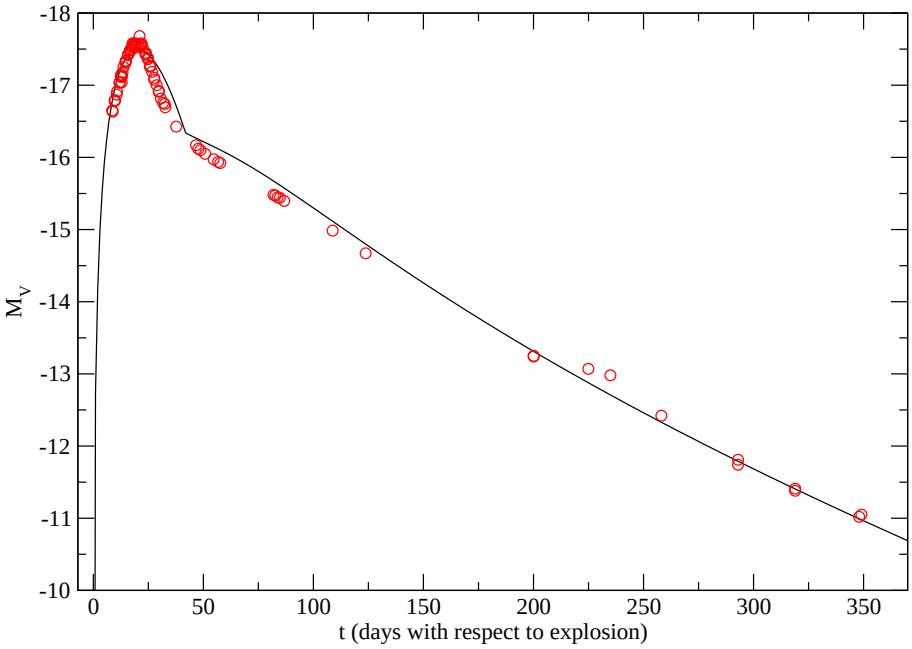

Figure 4.9: The best fit for SN 1993J; IIb

4.4.1 Type IIb

The only SE SN that has been observed early enough to see the break–out shock in the V–band LC is SN 1993J. The break–out shock has not been incorporated into the model and so that part of the data was left out of the SN 1993J fit. Figures 4.9 and 4.10 show the model fits for SNe 1993J and 1996cb, respectively. Both of the SNe IIb have somewhat large χ^2 values (Table 4.2) even though the model fits are fairly good. This is likely due to the relatively small uncertainties, δM_V. The area in the LC of SN 1993J where the fit is the worst is the late peak and early tail. This is also the area where the model assumptions are the poorest.

The values of E_k and M_{ej} determined here for SN 1993J are somewhat lower than those given by Young, Baron & Branch (1995) [96] and Blinnikov et al. (1998) [12]. The value of M_{Ni} matches well with these other studies.

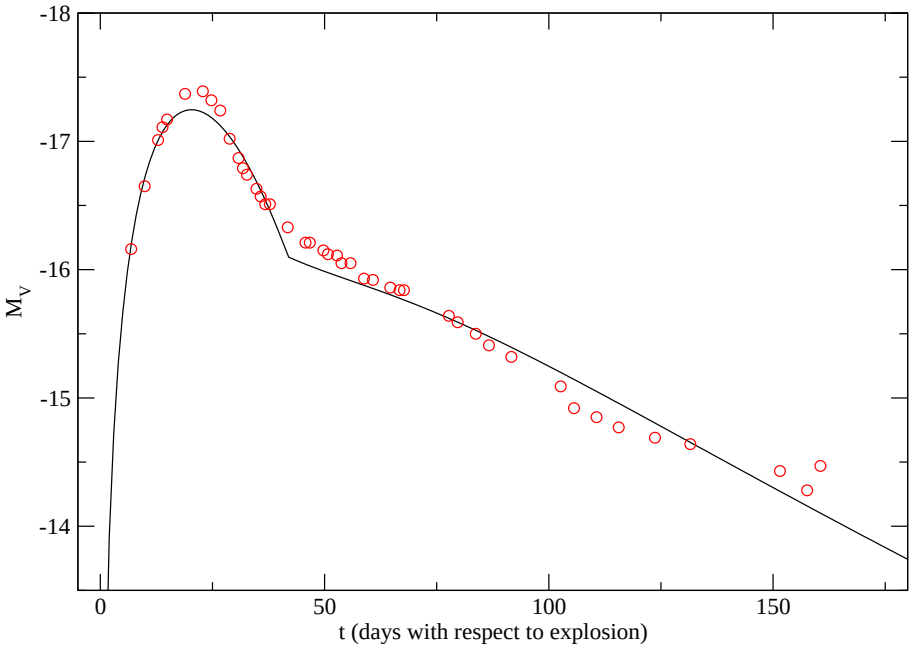

Figure 4.10: The best fit for SN 1996cb; IIb.

The model fit for SN 1996cb is a little too dim at the peak, but overall it is a pretty good fit. It has less E_k and M_{ej} than SN 1993J even though the two LCs line up pretty well (Figure 4.1). From looking at the spectra, we have determined that SN 1993J has a faster v_{phot}, and therefore a large E_k/M_{ej}, than SN 1996cb.

4.4.2 Type Ib

Of the six SNe Ib in the study only three have enough coverage in their LC to attempt a fit to the model. The model fits for these three (SNe 1983N, 1991D and 1999ex) are shown in Figures 4.11 – 4.13.

SN 1983N has a pretty good fit with relatively few points. It is the dimmest SN in the sample and therefore it has the lowest M_{Ni}. Shigeyama et al. (1990) [84] compared some model LCs to the SN 1983N data. Their models fixed E_k at 1 foe and varied the progenitor mass, which has a corresponding

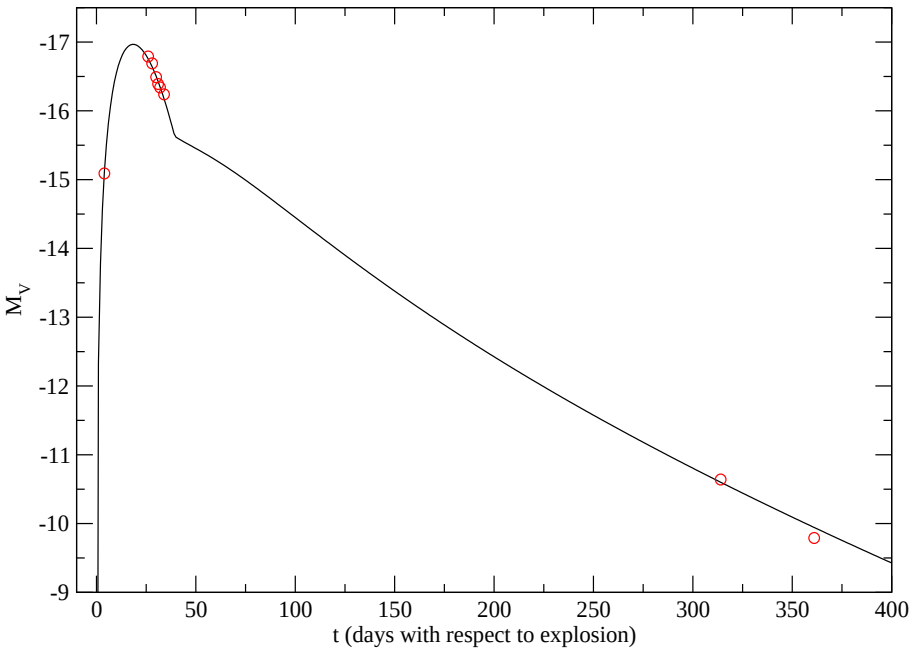

Figure 4.11: The best fit for SN 1983N; Ib.

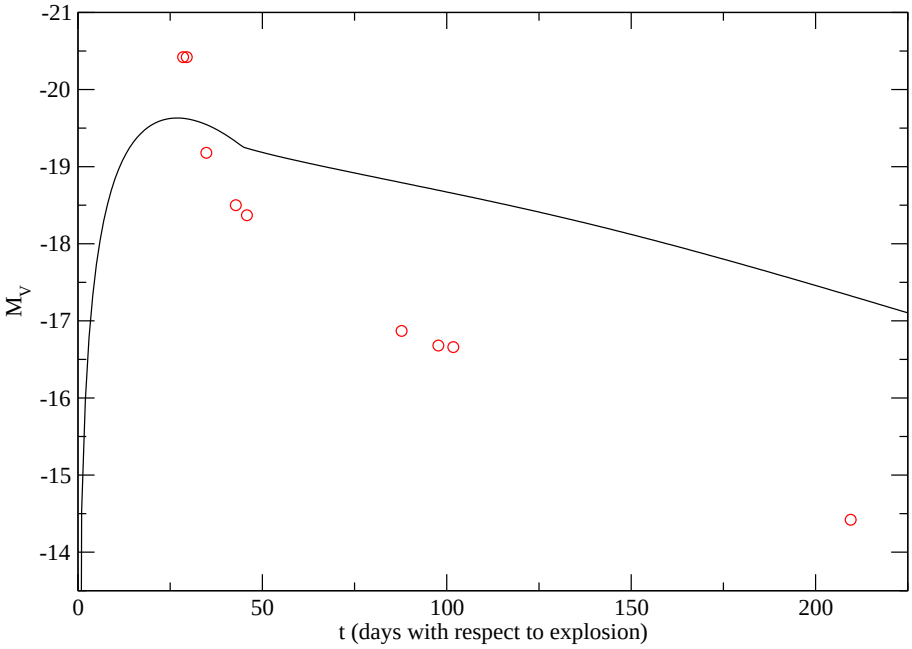

Figure 4.12: The best fit for SN 1991D; Ib.

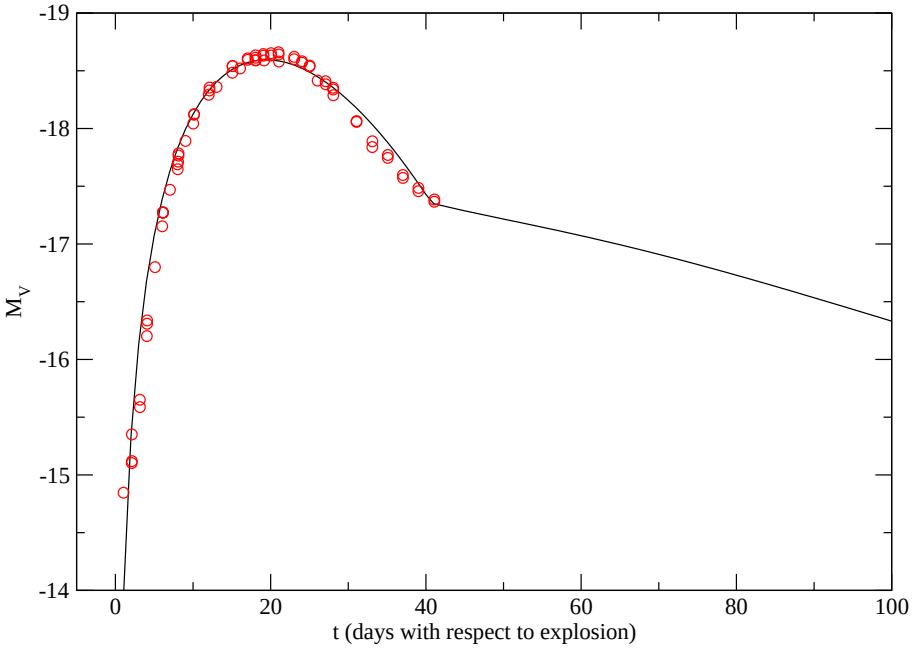

Figure 4.13: The best fit for SN 1999ex; Ib.

M_{ej}. The best fit to SN 1983N gave a progenitor mass of 4 $M_\odot$. From hydrodynamical calculations Shigeyama et al. (1990) [84] determine that the M_{ej} is 2.7 $M_\odot$, quite a bit higher than the value of 0.8 $M_\odot$ given in Table 4.2. We fixed the ratio of E_k/M_{ej}, allowing M_{ej} to vary, and hence E_k; rather than giving a specific value to E_k. When we fix E_k at 1 foe and allow M_{ej} to vary we get an M_{ej} of 1.3 $M_\odot$. This is higher than before, but still less than Shigeyama et al. (1990) [84].

SN 1991D is the brightest and also the most peculiar SN in the sample. Its LC falls extremely fast from the peak; although, from looking at its spectra, we have determined that E_k/M_{ej} for this SN is only 0.13 foe/$M_\odot$. This is the smallest in the sample. It's no wonder the model has a hard time reconciling these two, seemingly contradictory, aspects. The M_{Ni} is given in Table 4.2 as $\geq$1.52. An upper limit to the M_{Ni} was set at 80% of the M_{ej} in the program.

This prevented the program from searching for ridiculously high values of M_{Ni}. SN 1991D is the only SN in the sample to actually reach this limit.

It is possible to get a good fit for SN 1991D if we allow E_k to vary as a free parameter. The fit is pretty good, although the resulting E_k/M_{ej} ratio is about 8 foe/$M_\odot$; which is not what we see in the spectra. The peak magnitude for this fit is around -21.

Benetti et al. (2002) [9] took a different approach to SN 1991D. They considered the idea of an exploding white dwarf inside the envelope of a helium star, or giant companion, during a common–envelope phase. This would essentially be a SN Ia inside a helium envelope. They argue that the large radius of the helium envelope would produce the high peak luminosity, while the small envelope mass would result in a very fast decline after peak. They show that, except for the brightest points, the LC would closely resemble that of the Type Ia SN 1994D. The helium in the spectra would be accounted for as well.

SN 1999ex has very good coverage around the peak of the LC. Unfortunately, there are no data for the tail. As for the peak, the model fits quite well. It has a relatively low E_k, but one that is comparable to the other SNe Ib.

4.4.3 Type Ic

Model fits were done for 10 SNe Ic LCs; three of which are considered hypernovae. The SNe Ic LC fits are shown in Figures 4.14 – 4.23. The fit for SN 1962L is good, but there are only data available near peak. It has the lowest E_k in the sample. The M_{Ni} is more than half the M_{ej}. The χ^2 is very low due to the large uncertainty of $\delta M_V = 0.85$.

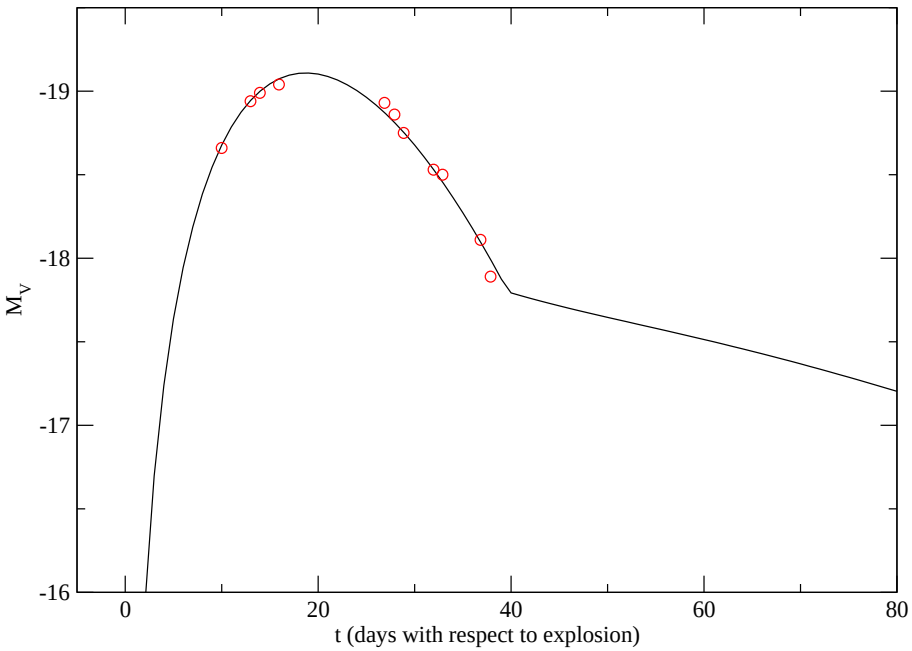

Figure 4.14: The best fit for SN 1962L; Ic.

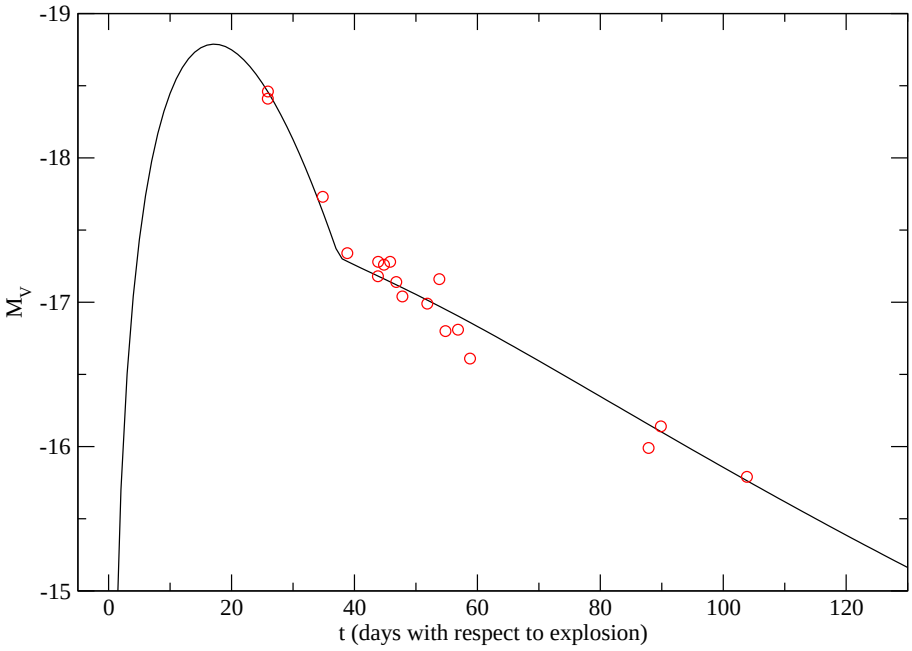

Figure 4.15: The best fit for SN 1983I; Ic.

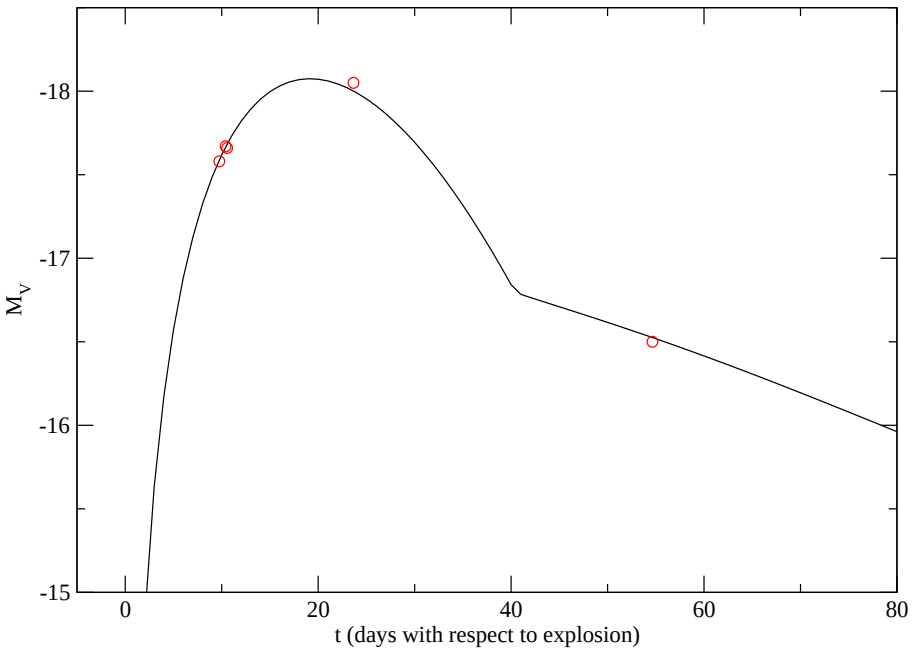

Figure 4.16: The best fit for SN 1983V; Ic.

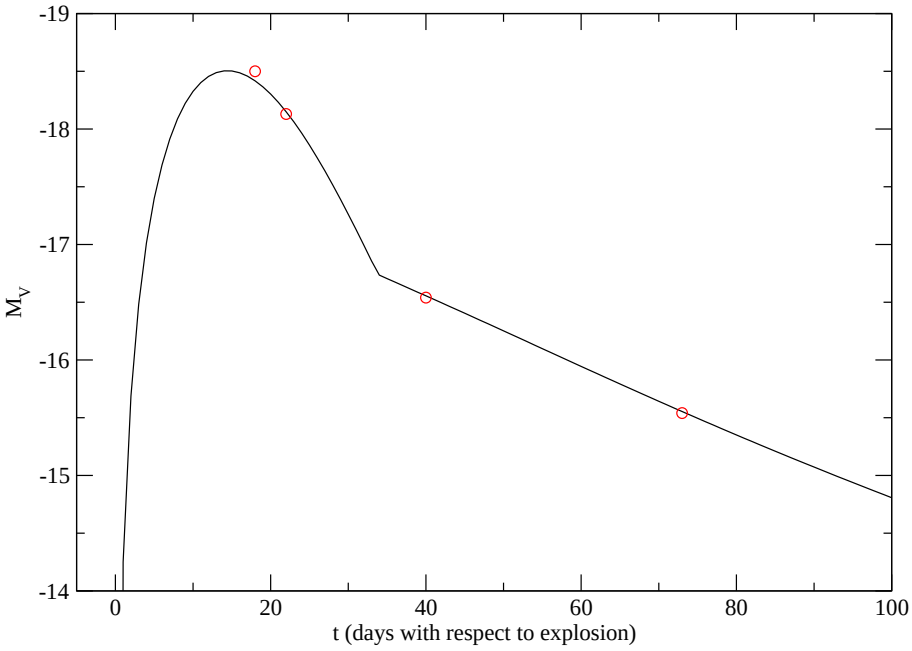

Figure 4.17: The best fit for SN 1987M; Ic.

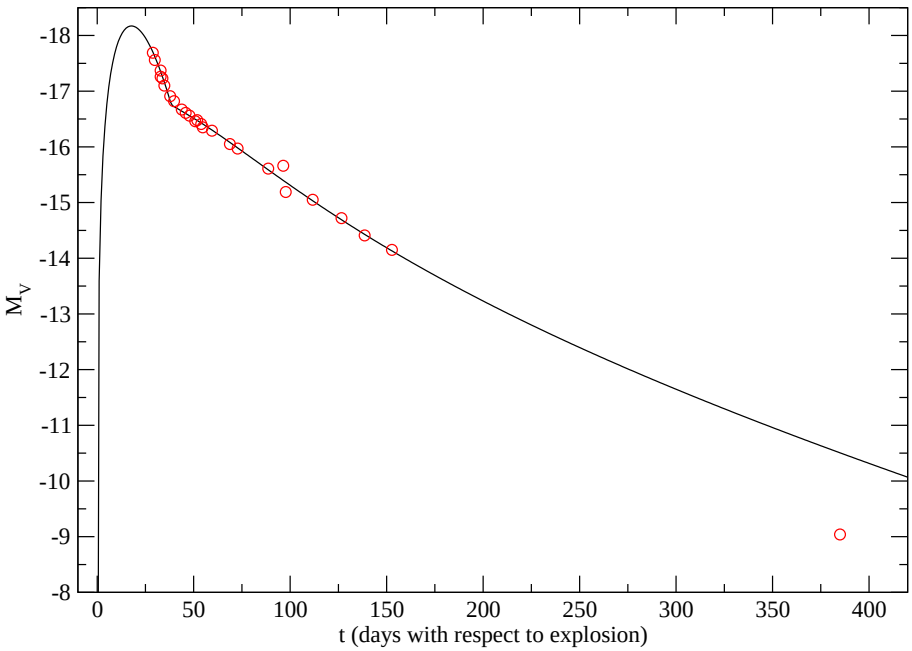

Figure 4.18: The best fit for SN 1990B; Ic.

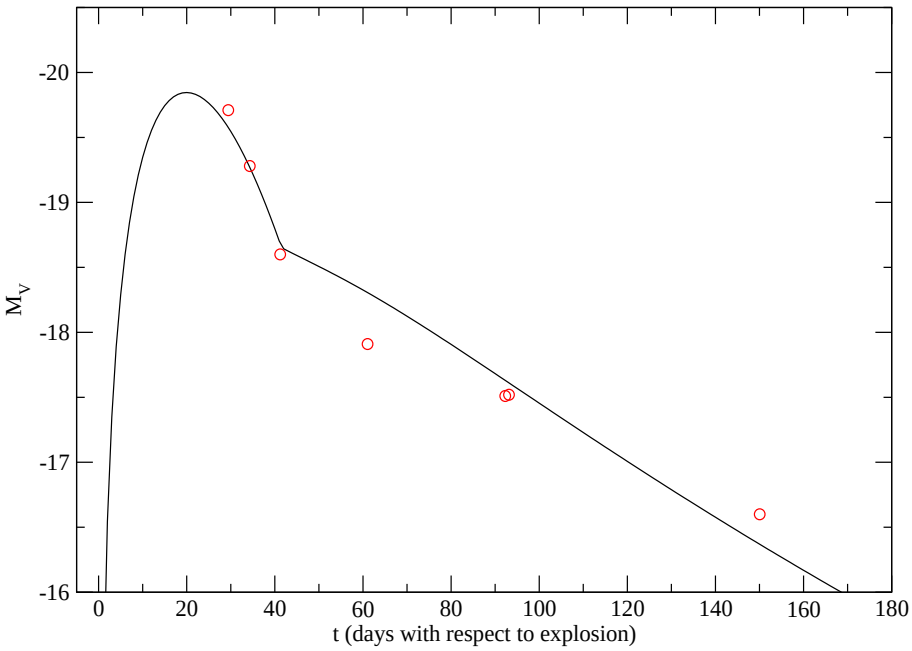

Figure 4.19: The best fit for SN 1992ar; Ic.

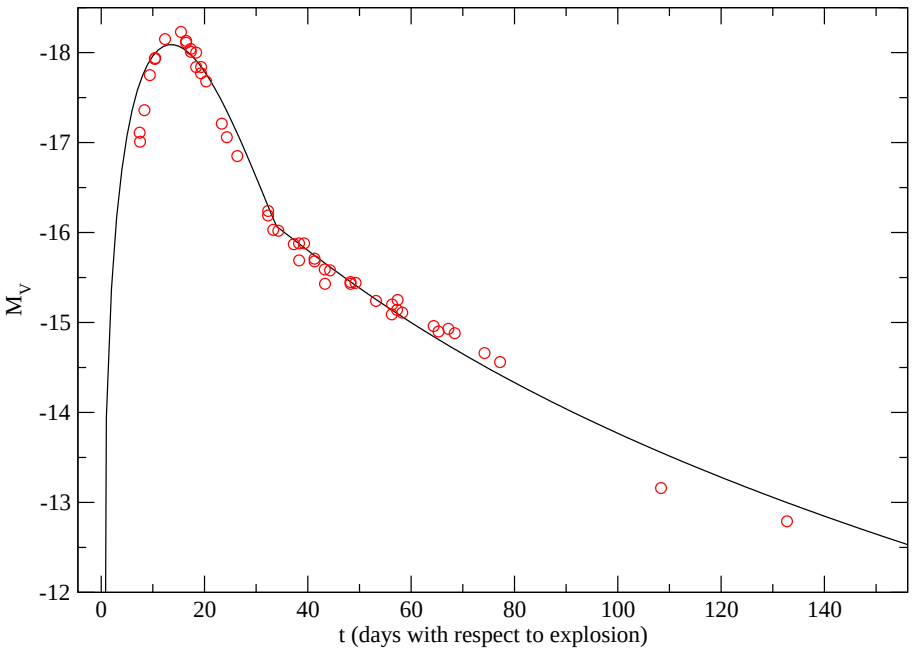

Figure 4.20: The best fit for SN 1994I; Ic.

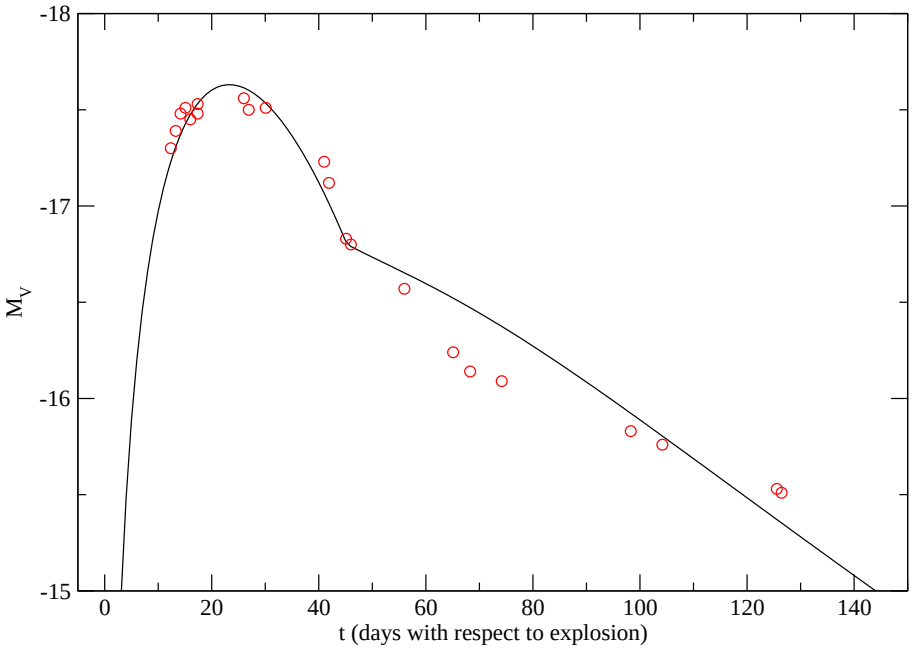

Figure 4.21: The best fit for SN 1997ef; Ic hypernova.

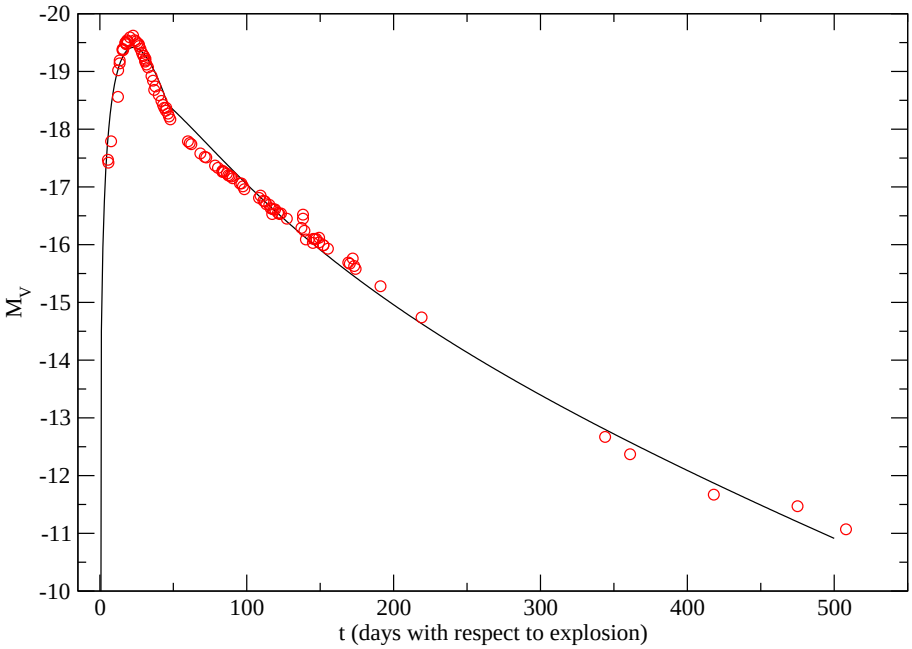

Figure 4.22: The best fit for SN 1998bw; Ic hypernova.

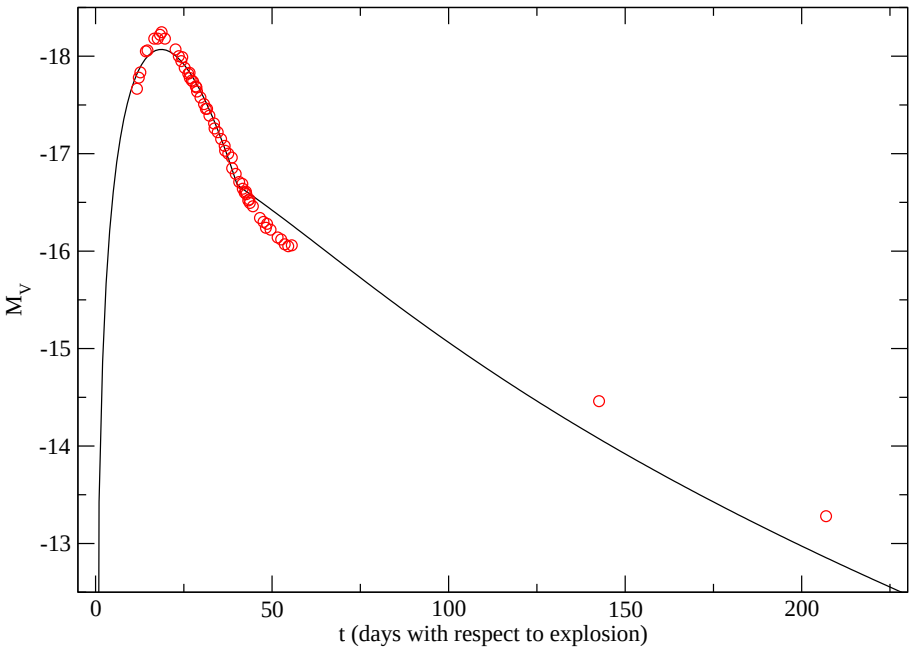

Figure 4.23: The best fit for SN 2002ap; Ic hypernova.

The data for SN 1983I are rather scattered in the tail and there are no pre–peak data. The fit is about as good as can be expected. In the same paper as mentioned above for SN 1983N, Shigeyama et al. (1990) [84] also looked at SN 1983I. Their best fit lead to an M_{ej} of 2.1 $M_\odot$; compared to our value of 0.7 $M_\odot$. When we fixed E_k to 1 foe and varied M_{ej}, we got 1.1 $M_\odot$ for M_{ej}. Once again this is more than before but less than Shigeyama et al. (1990) [84].

Usually two SNe with the same M_{Ni} have about the same brightness. In the case of SNe 1983V and 1987M they both have about the same M_{Ni}, but SN 1987M is half a magnitude brighter. This is because SN 1987M has a significantly lower M_{ej} allowing it to rise to peak faster, and brighter, than SNe 1983V without requiring more nickel. Nomoto et al. (1990) [64] produced model LCs for SN 1987M. It appears that they also fixed E_k to 1 foe and their best fit lead to an M_{ej} of 2.1 $M_\odot$. When we set E_k to 1 foe we get $M_{ej} = 0.8$ $M_\odot$, compared to 0.4 $M_\odot$ when E_k/M_{ej} is fixed.

SN 1990B has quite a few points and fits the model well, although there are no pre–peak data. According to Clocchiatti et al. (2001) [22] the last point is likely confused with host galaxy light. SN 1992ar is the brightest SN Ic in the sample and as such has the highest M_{Ni}. SN 1994I has a very fast LC and the model fit was too broad at peak. Because of this, the value of t_{rise} given in Table 4.2, which is already the smallest, is too large. It makes sense, then, that SN 1994I has the largest E_k/M_{ej} ratio of any normal SN Ic in the sample; where according to Young, Baron & Branch (1995) [96] that value is 1.1 foe/$M_\odot$.

The last three LCs (Figures 4.21 – 4.23) are the hypernovae. As mentioned above, these are SE SNe that are very energetic (see Table 4.2). The LC data

for SN 1997ef are very broad at peak and appear to have a very late transition point. It is difficult to get a good fit to this data. Iwamoto et al. (2000) [40] had a very similar looking fit with their numerical model; although their E_k, at 8 foe, was somewhat larger than the 3.26 foe found here. In both cases SN 1997ef is quite energetic but still not very bright. In fact it is the dimmest SNe Ic in the sample.

SN 1998bw, on the other hand, is very bright for a SN Ic. The model fit shown in Figure 4.22 is pretty good. The time where the model fit is the worst is near the transition point where the model assumptions are the poorest. The E_k value of 31 foe determined here is the largest in the sample. This is not unexpected. Nakamura et al. (2001) [63], generating synthetic LCs numerically, had a 30 foe model LC and a 50 foe model LC. The 50 foe model LC had the best fit. Woosley, Eastman & Schmidt (1999) [94] found the best fit to be 22 foe with their model.

Figure 4.23 shows the fit for SN 2002ap. Overall it is pretty good, although the peak is a little dim in the model and the transition point is somewhat early. The model clearly has trouble finding a tail that fits both the transition point and the two late time data points. If there were more points in the tail, to more evenly weight the χ^2, the fit might be better. The small nickel mass shown in Table 4.2 for both SN 2002ap and SN 1997ef reflects well the relatively dim peak brightness for their respective LCs. Model fits were carried out by Mazzali et al. 2002 [59] for SN 2002ap. They determined E_k to be about 4 – 10 foe and M_{ej} to be about 2.5 – 5 $M_\odot$. Their value of M_{Ni} is 0.07 $M_\odot$. This is compared to our values of $E_k = 2.72$ foe, $M_{ej} = 1.7$ $M_\odot$ and $M_{Ni} = 0.14$ $M_\odot$.

4.5 Summary

There were two SNe IIb, three SNe Ib and 10 SNe Ic (three of which are hypernovae) that are fit to the LC model. While the two SNe IIb have similar LCs, their E_k/M_{ej} ratios were different and therefore their model fits produced different E_k values.

Of the three SNe Ib, only two of them had reasonable fits. SN 1991D is just too peculiar to be fit by such a standard LC model. The other two SNe Ib (SNe 1983N and 1999ex) have very similar E_k and M_{ej} values, although their different M_{Ni} reflect their noticeably different peak magnitudes.

The normal SNe Ic have a variety of parameter values. This is definitely not a homogeneous group. The E_k varies from 0.11 foe for SN 1962L to 1.14 foe for SN 1992ar. The M_{ej} varies from 0.4 $M_\odot$ for SN 1987M to 1.5 $M_\odot$ for SN 1992ar. The M_{Ni} varies from 0.08 $M_\odot$ for SN 1994I to 0.84 $M_\odot$ for SN 1992ar. At the high end of the range for each of these parameters is SN 1992ar. SN 1992ar is brighter than any SE SN in the study (including hypernovae) except for the very peculiar SN 1991D.

As expected, all hypernovae have considerably more E_k than the normal SE SN. Their M_{ej} are also higher, but their M_{Ni} vary according to their differing peak magnitudes.

Values of M_{ej} (and E_k) are consistently lower than those of other models (Shigeyama et al. 1990 [84] and Nomoto et al. 1990 [64]), while values for M_{Ni} are a little higher. Even with this, good fits are produced. These other models use M_{ej} determined from hydrodynamical calculations of exploding helium stars

with certain masses. They also impose a kinetic energy of 1 foe. The model used here, on the other hand, uses the constraint of E_k/M_{ej}; so if M_{ej} is low, E_k will be low. A lower E_k makes the LC dimmer. Because the M_{Ni} is directly correlated with peak brightness, the slightly higher M_{Ni} compensates, allowing the model LC to be bright enough.

Chapter 5

Gamma–Ray Burst Optical After–Glow Light Curves

5.1 Introduction

It has been suspected for some time that Gamma–Ray Bursts (GRBs) and SNe were related, but this had not been shown conclusively until 2003. This is when spectra of the optical afterglow (AG) of GRB030329 showed broad spectral features like those found in the spectra of hypernovae (Garnavich et al., 2003 [34]). In fact, these spectra showed a remarkable similarity to the spectra of SN 1998bw, a SN Ic hypernova within the error bars of GRB980425. At this time even the critics began to agree that there was a connection between GRBs and SNe. The SN associated with GRB030329 was given the name SN 2003dh. Other likely SN/GRB connections are SN2002lt/GRB021211, SN2001ke/GRB011121 and SN1997cy/GRB970514.

There is general agreement that a GRB occurs when the core of a massive star collapses and a black hole is formed. A short lived accretion disk forms around the black hole accompanied by two relativistic polar jets. The gamma–rays are emitted by the jets in the general polar direction.

Beyond this there is disagreement as to how the black hole is formed. The two most prominent models are the Collapsar and the Supranova models. The initial Collapsar model (MacFadyen & Woosley, 1999 [53]) involves the direct formation of a black hole after the core–collapse of a massive star. An outward shock fails to form and everything outside the core falls in toward the black hole. An accretion disk forms along with the relativistic jets. The jets only last for a few seconds; as long as there is a strong enough accretion rate ($\sim$ 0.001 – 0.01 $M_\odot$ s^{-1} according to MacFadyen, Woosley & Heger, 2001 [54]).

MacFadyen, Woosley & Heger, 2001 [54] expanded the Collapsar model to also include a delayed formation of a black hole. The original model is now called a Type I Collapsar (with the direct formation of a black hole) and the model with the delayed formation of a black hole is called a Type II Collapsar. The massive star core–collapse that leads to a Type II Collapsar first produces a neutron star. An outgoing shock forms and a SN occurs. Some of the material deep inside the ejecta fails to escape the neutron star and falls back. This extra mass causes the neutron star to collapse to a black hole. An accretion disk forms as well as the relativistic jets. The neutron star can last from a few minutes to 1 – 2 days (Dermer, 2004 [23]) before collapsing to a black hole. The Type I Collapsar model also allows for a SN to occur along with the direct formation of a black hole.

The Supranova model (Vietri & Stella, 1998 [92]) is similar to the Type II Collapsar, except that there is no fall–back material. Instead, the newly formed neutron star is over the upper mass limit for a neutron star, but it has enough angular momentum to provide centrifugal support against collapse. The neutron

star loses energy through magnetic dipole radiation at a rate of about four times greater than the Eddington luminosity [92]. When enough angular momentum is lost the neutron star collapses to a black hole. This model allows for a much longer delay in the formation of the black hole than with the Type II Collapsar. In this case there could be days, or weeks, before the neutron star collapses (Dermer, 2004 [23]).

If a neutron star exists for days, or weeks, after the SN then there should be observable X–ray radiation from the interaction between the strong neutron star winds and the SN shell material. The X–ray spectrum would have a distinctive signature; mainly the ^{56}Fe Kα feature. The observed X–ray spectra of GRBs do not yet, conclusively, show these features. The Swift orbital observatory, due to be launched in late 2004, will have much higher resolution than previous orbital observatories and should be able to detect the signature if it is there.

The GRB AG data used here, and the method applied to the data for separating out the SN component, are discussed in §5.2. The LC model fits and their results are covered in §5.3. A summary is given in §5.4.

5.2 Data

The GRB AG data used here are from Zeh, Klose & Hartmann (2003) [98]. They model the AG light curves of seven GRBs. The model takes into account three components: light from the host galaxy, AG light from the jet and SN light. The AG light from the jet is modeled by a broken power law. The SN light is based on the LC of SN 1998bw. Assuming there is a continuous distribution from the LC of one filter to another for SN 1998bw, an appropriately redshifted

LC can be generated. Two free parameters were used to adjust the SN LC for the best fit. One adjusts the overall brightness and the other is a stretch factor. Adding these components together they were able to successfully reconstruct the observed LCs.

What we have done is to take the observed R–magnitude data from Zeh, Klose & Hartmann (2003) and subtract off the AG light and galaxy light. Then, using spectra of SN 1998bw, we calculated K–corrections in order to convert the redshifted R magnitudes back to rest frame V magnitudes. Once this was done, the apparent V magnitudes were converted to absolute magnitude in the same manner discussed in Chapter 3. Foreground extinction from Schlegel, Finkbeiner, & Davis (1998) [82] has been taken into account by Zeh, Klose & Hartmann (2003) for the R–magnitudes. Host galaxy extinction is very difficult to determine. When mentioned in the literature, it is almost always model dependent. For this reason it is not included here.

The peak data used (K–correction, V apparent magnitude, distance modulus and absolute magnitude) are given with their uncertainties in Table 5.1. Luminosity distances are calculated in the same manner as in Chapter 3; using redshifts from Zeh, Klose & Hartmann (2003). The peak absolute magnitudes are all in a rather small range between about -19 and -20 magnitudes. This could possibly be a selection effect due to fact that if there are any dim SNe associated with GRBs their light would likely be lost in the bright light of the AG.

GRB	K_{VR}*(98bw)*	*V*	μ	M_V
970228	0.11 ± 0.88	24.50 ± 0.91	43.463 ± 0.003	-18.96 ± 0.91
990712	-0.27 ± 0.58	23.11 ± 0.59	42.224 ± 0.005	-19.11 ± 0.59
991208	0.11 ± 0.90	23.45 ± 0.92	43.504 ± 0.006	-20.05 ± 0.92
010921	-0.08 ± 0.60	22.86 ± 0.64	42.328 ± 0.005	-19.47 ± 0.64
011121	-0.24 ± 0.49	22.24 ± 0.57	41.764 ± 0.006	-19.52 ± 0.57
020405	0.09 ± 0.89	23.40 ± 0.91	43.463 ± 0.016	-20.06 ± 0.91

Table 5.1: Data used for determining the peak SN absolute magnitudes. Foreground extinction is included but not host galaxy extinction.

Values of K_{VR} were looked at for three hypernovae (SNe 1997ef, 1998bw and 2002ap). The spread in these values was used in determining the uncertainties in K_{VR}. The uncertainties in V, and therefore M_V, are dominated by the uncertainties in K_{VR}.

The resulting LC data are shown in Figure 5.1. Only data points near peak are used here. Very early data points are not used because SN 1998bw spectra are not available for the K–corrections. The late–time data points are not used because they are too difficult to separate from the galaxy light.

5.3 Results

The model described in Chapter 4 is used with the GRB data. Early–time spectra are required to get the E_k/M_{ej} values for each SN. Due to the lack of spectra available, E_k/M_{ej} could not be calculated for this sample.

We calculated $E_k/M_{ej} = 5.21$ foe/$M_\odot$ for SN 2003dh using the method described in Chapter 4. This is in relatively good agreement with Mazzali et al. (2003) [60] who concluded that $E_k = 38$ foe and that $M_{ej} = 8\ M_\odot$ giving us $E_k/M_{ej} = 4.75$ foe/$M_\odot$.

Because Zeh, Klose & Hartmann (2003) were so successful in reconstructing

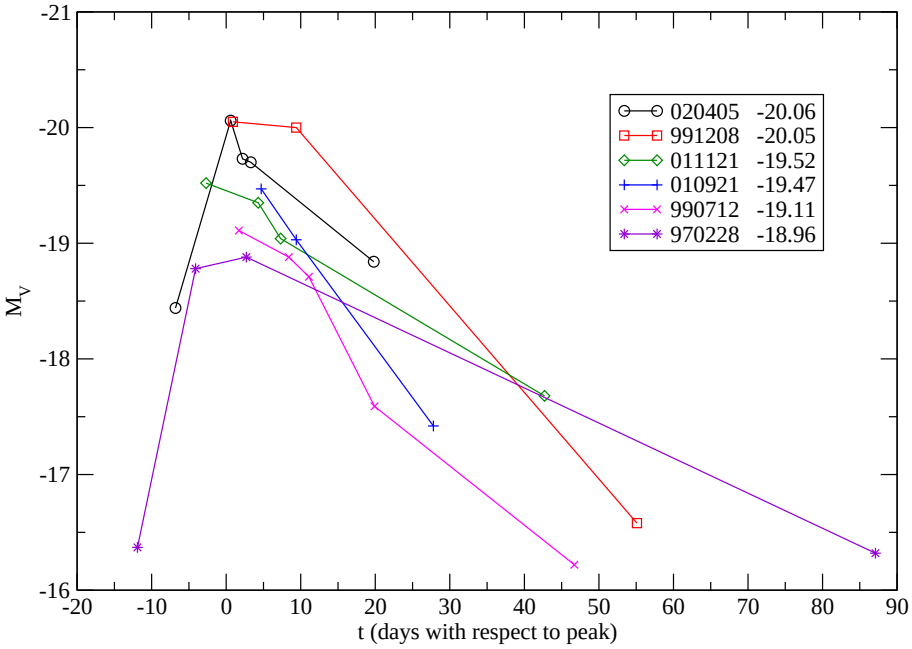

Figure 5.1: Observational data with the GRB AG and host galaxy light subtracted out. Host galaxy extinction is not included. Lines are only to guide the eye.

the total AG LC using the SN 1998bw LC, and the fact that the spectra of SN 2003dh so closely resembles that of SN 1998bw, we can adopt the E_k/M_{ej} value of 5 foe/$M_\odot$ with reasonable confidence for our sample. This, of course, would be under the assumption that all SN components of GRBs resemble the only two SNe for which we have good spectra.

One drawback to this analysis is that there are so few points in each LC. The points we have are fairly well distributed in time. All of the LCs have data both before and after the transition point (except for GRB020405) and nearly all have points at or before peak. Because of this, it is worth carrying out the analysis.

The model fits are shown in Figures 5.2 – 5.7. All of the LCs have good fits to the model, and their parameter values are listed in Table 5.2. The very small

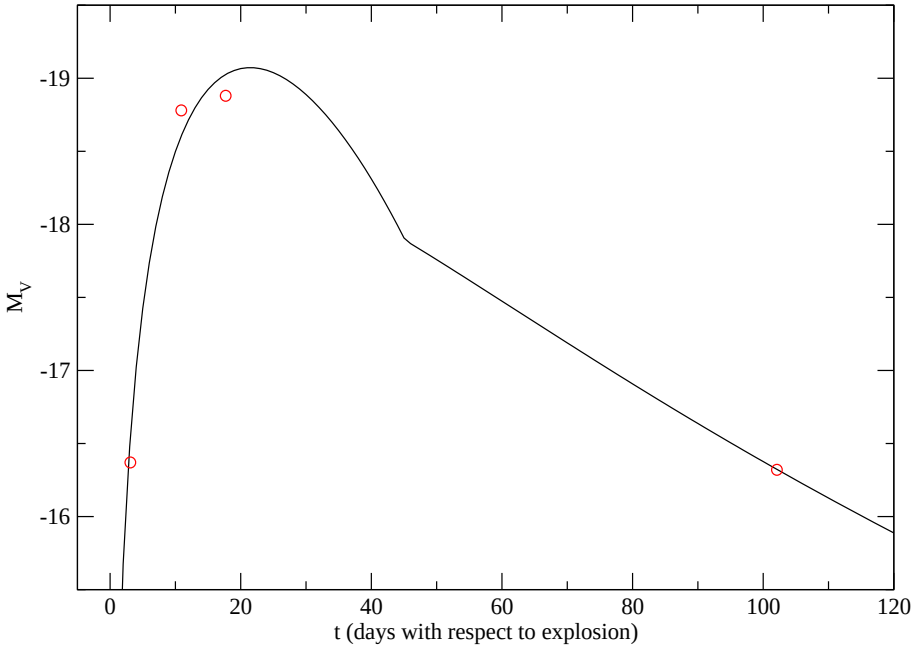

Figure 5.2: The best fit for the SN component of GRB970228.

χ^2 values are, mostly, due to the high uncertainties in M_V. These uncertainties are different from those in Table 5.1 because these uncertainties contain the uncertainty in E_k/M_{ej} used in the model.

GRB	E_k *(foe)*	M_{ej} $(M_\odot)$	M_{Ni} $(M_\odot)$	t_{rise} *(days)*	χ^2_r	δM_V *(mag)*	N
970228	25.0	5.0	0.49	21	2.37E−2	1.01	4
990712	9.5	1.9	0.30	16	5.84E−3	0.73	5
991208	6.5	1.3	0.60	14	9.99E−5	1.02	3
010921	9.5	1.9	0.53	16	8.88E−5	0.77	3
011121	25.0	5.0	0.81	21	4.65E−3	0.71	4
020405	8.0	1.6	0.55	15	4.12E−2	1.01	5

Table 5.2: Parameter values from the best χ^2 fit of the model to the data for the SN component of the GRB afterglow.

All of the energies listed in Table 5.2 are quite high; which is expected because of the assigned hypernova E_k/M_{ej} value given to SNe here. Two of the SNe have $E_k = 25$ foe (GRB970228 and GRB011121). The lowest E_k is 6.5 foe (GRB991208). The nickel masses range from 0.30 $M_\odot$ for GRB990712 to 0.81

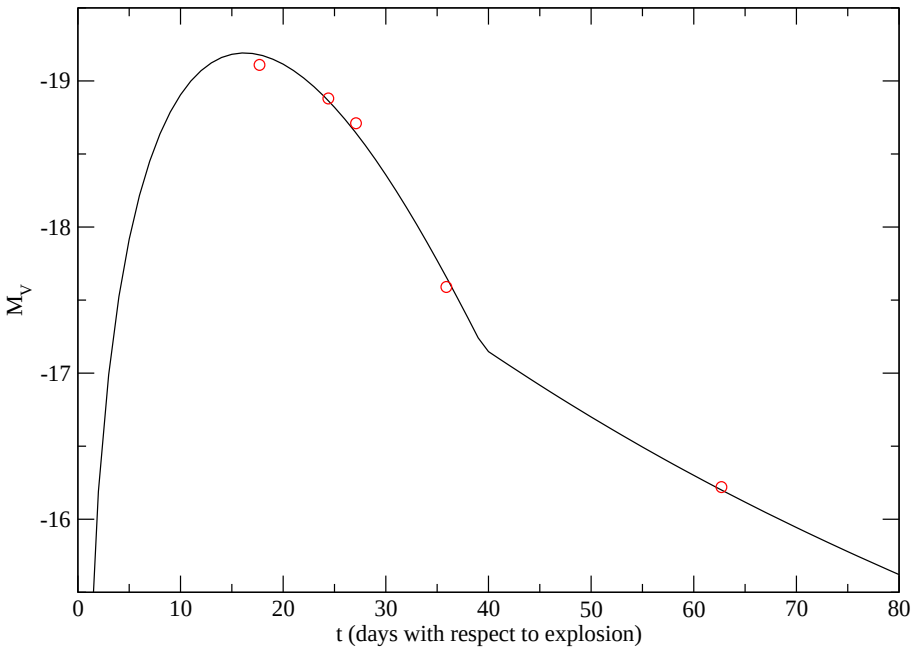

Figure 5.3: The best fit for the SN component of GRB990712.

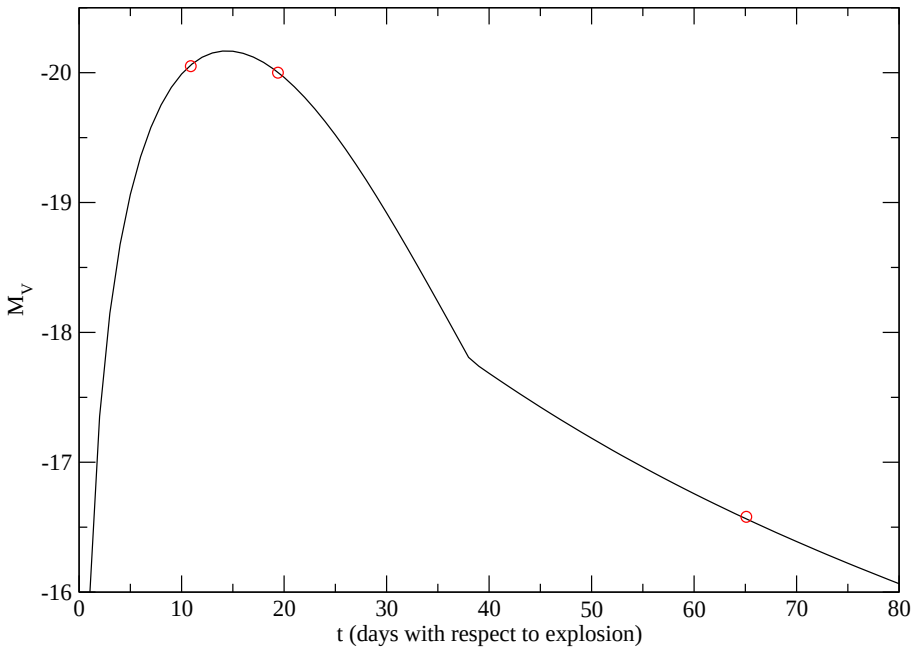

Figure 5.4: The best fit for the SN component of GRB991208.

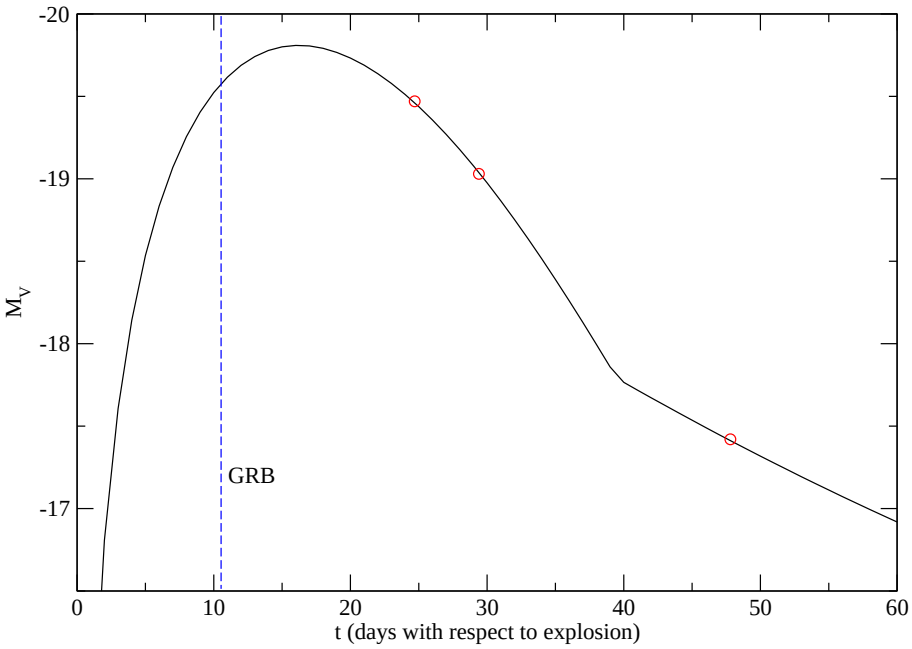

Figure 5.5: The best fit for the SN component of GRB010921.

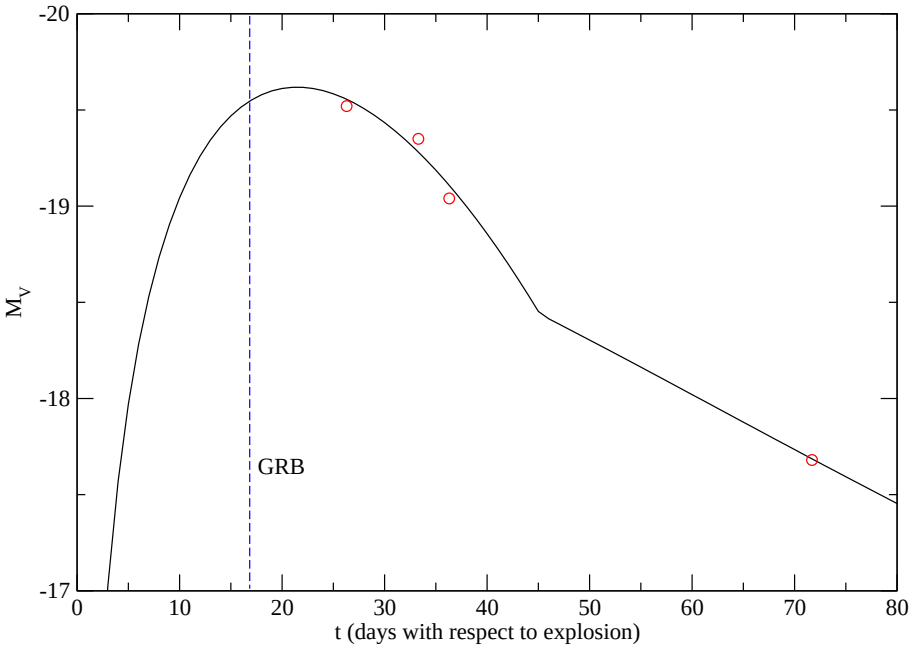

Figure 5.6: The best fit for the SN component of GRB011121.

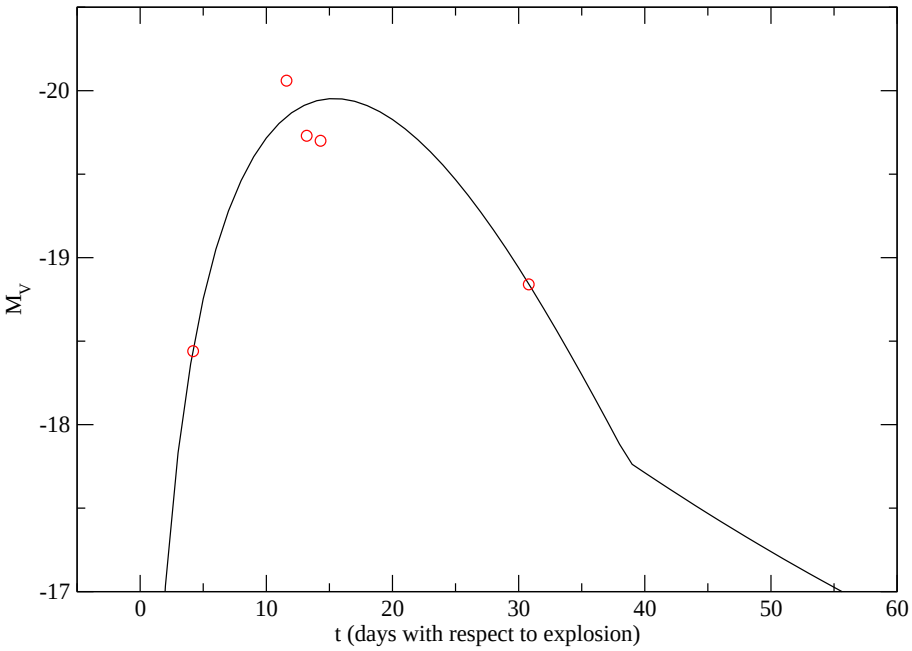

Figure 5.7: The best fit for the SN component of GRB020405.

$M_\odot$ for GRB011121. The rise times range from 14 days for GRB991208 to 21 days for GRB970228 and GRB011121. On the high end of these parameters is GRB011121, although it is about average in brightness.

All but two of the SNe in this sample are determined to have occurred within a week of the associated GRB. The vertical dashed lines in Figures 5.5 and 5.6 represent the time of the GRB for GRB010921 and GRB011121, respectively. The SN of GRB010921 is found to have occurred 10.5 days before the GRB, while the SN of GRB011121 is found to have occurred 16.8 days before the GRB. This supports the Supranova model for at least some of the GRBs. Critics of the Supranova model point out that the necessary X–ray signature, mentioned in §5.1, has not yet been, unambiguously, detected.

In order to check our result we decided to see what the fit would look like if we forced the explosion date of the SN to coincide with the GRB date ($t_{SN} = t_{GRB}$).

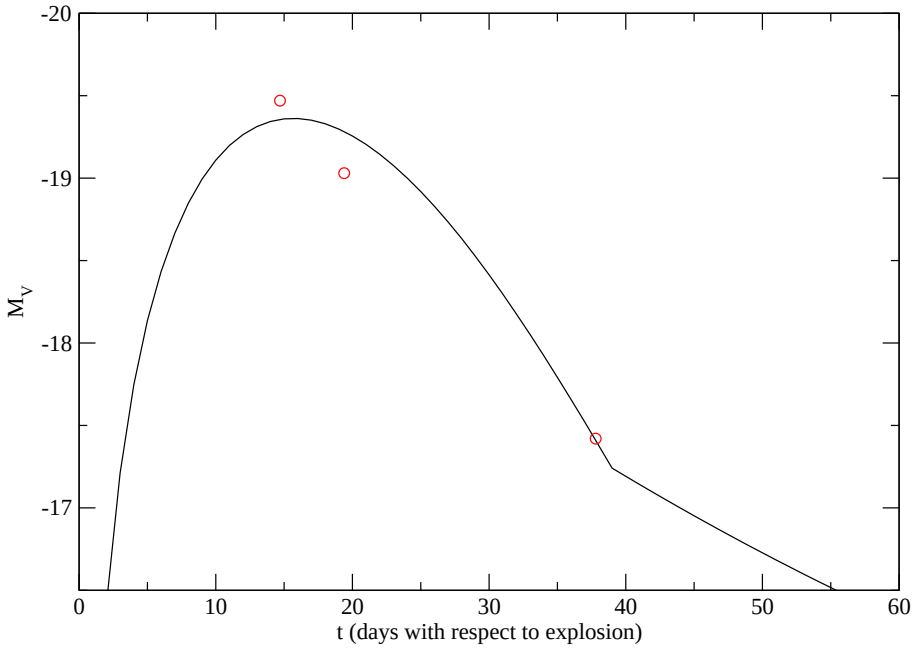

Figure 5.8: The best fit for the SN component of GRB010921 when t_{SN} is forced to equal t_{GRB}.

The fits are shown in Figures 5.8 and 5.9 for GRB010921 and GRB011121, respectively. The fit for GRB010921 isn't too bad, but its certainly worse than Figure 5.5. The fit for GRB011121, on the other hand, is very bad. We then decided to make E_k a free parameter to see if allowing E_k and M_{ej} to vary independently would improve the fits. With this change the fits looks the same as they did before. Making E_k a free parameter didn't help.

5.4 Summary

We found that when subtracting out the AG light of the jet (and host galaxy light) we are left with a LC that resembles a SN light curve and can be modeled as such. These SNe are found to be in a relatively narrow peak absolute magnitude range; but this is thought to be due to a selection effect. The kinetic energies, here, range from 6.5 – 25 foe, which is significantly more than with

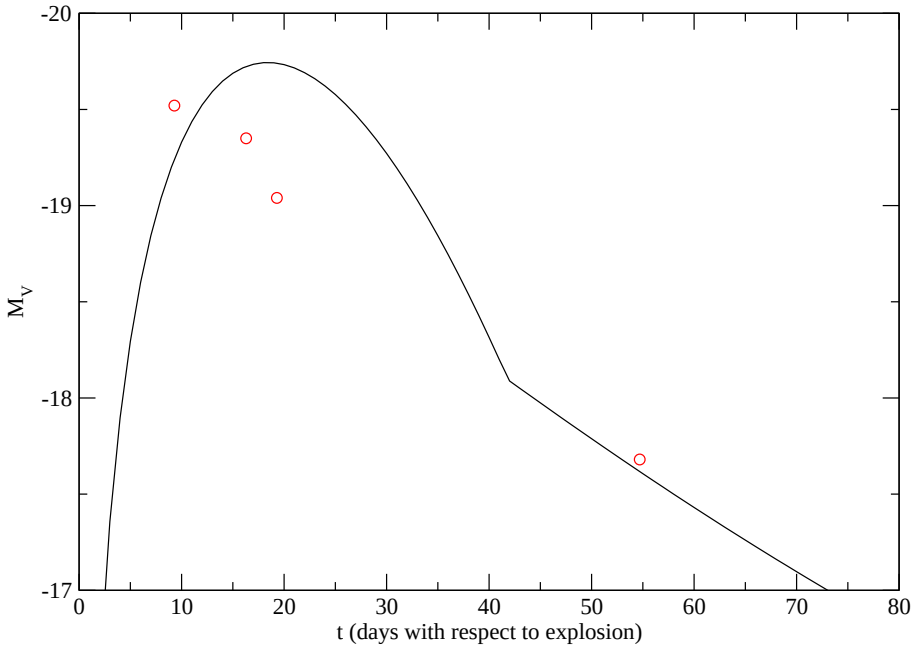

Figure 5.9: The best fit for the SN component of GRB011121 when t_{SN} is forced to equal t_{GRB}.

normal SE SNe. Nickel masses range from 0.30 – 0.81 $M_\odot$. In two of the SNe presented here we find that they occur significantly (more than a week) before the associated GRB.

Chapter 6

Conclusions

The SUSPECT supernova data archive fills a need in research and is potentially, very useful in education. Most of the data used in this dissertation are in the SUSPECT database.

The peak absolute–magnitude distribution of the current SE SNe sample is presented and displays a broad range. It does not appear to fit either a single or double peak Gaussian distribution. Even though SNe Ib are, on average, dimmer than SNe Ic there are not enough data available yet to determine different distributions for SNe Ib and Ic. There are, however, a few SE SNe that are noticeably brighter than the others, there are not enough data to say conclusively that they are from a separate population. Those with peculiar spectra are found among both the normal and the bright SNe. Those with normal spectra are also found among both the normal and the bright SNe.

The light curves of SE SNe are compared and modeled. These LCs vary greatly, and this is reflected in the model parameter values found. SNe Ib range from the dimmest (SN 1983N) SN in the study to the brightest (SN 1991D). SN 1991D is likely one of the most peculiar SNe every studied. Among the SNe Ic we see a lot of variation in peak brightness and light curve width near

peak. It is clear that, while spectroscopically normal, SN 1994I does not have a typical light curve. It is much faster than any other SE SN, with the possible exception of SN 1991D. On the high end of the parameter values for for normal SE SNe is SN 1992ar. It is the brightest SN in the study except for SN 1991D. The hypernovae were all found to have significantly higher E_k than the normal SE SNe; which is to be expected.

Light curves of the SN component in a few GRB afterglows are compared and modeled. All of them fit quite well to the model and show high kinetic energy, as expected. Two of the SNe in the sample are shown to have occurred more than a week before their associated GRB. This supports the Supranova model for at least some GRBs. The hypernovae found with GRBs and without GRBs pose a problem for high redshift SN Ia searches. These searches produce large samples of, what are hoped to be, SNe Ia. Core–collapse SNe are usually thought to be too dim to significantly contaminate the samples. Hypernovae, and even some normal SE SNe, are shown to be just as bright as SNe Ia. These bright core–collapse SNe can be discerned from SNe Ia by spectra; but spectra are usually not practical for high–redshift SNe. It has been shown (Poznanski et al. 2002[71]) that colors taken from good quality photometry of various epochs can be used to separate the SNe Ia from the rest. This is what will need to be done.

Bibliography

[1] Allen, C. W. 2000, *Allen's Astrophysical Quantities*, ed. Cox, A. (Fourth Edition; New York: Springer–Verlag)

[2] Arnett, D. 1980, ApJ, 237, 541

[3] Arnett, D. 1982, ApJ, 253, 785

[4] Ayani, K., R. Furusho, R., Kawakita, H., Fujii, M., & Yamaoka, H. 1999, IAUC7244

[5] Barbon, R., Benetti, S., Cappellaro, E., Patat, F., Turatto, M., & Iijima, T. 1995, A&AS, 110, 513

[6] Barbon, R., Buondi, V., Cappellaro, E., & Turatto, M. 1999, A&AS, 139, 531

[7] Barth, A. J., van Dyk, S., Filippenko, A., Leibundgut, B., & Richmond, M. 1996, AJ, 111, 2047

[8] Benetti, S., Cappellaro, E., Turatto, M., & Pastorello, A. 2000, IAUC7375

[9] Benetti, S., Branch, D., Turatto, M., Cappellaro, E., Baron, E., Zampieri, L., Della Valle, M., & Pastorello, A. 2002, MNRAS, 336, 91

[10] Bertola, F. 1964, Ann. Astrophys., 27, 319

[11] Bessel, M. 1990, PASP, 102, 1181

[12] Blinnikov, S., Eastman, R., Bartunov, O., Popolitov, V., Woosley, S. 1998, ApJ, 496, 454

[13] Bloom, J., Frail, D., & Kulkarni, S. 1998, IAUC6899

[14] Branch, D., et al. 2002, ApJ, 566, 1005

[15] Branch, D. 2003, *A Massive Star Odyssey, from Main Sequence to Supernova*, Proc. IAU Symposium NO 212, eds. K. A. van der Hucht, A. Herrero, & C. Estaban (San Francisco: Astronomical Society of the Pacific), p. 346

[16] Buras, R., Rampp, M., Janka, H., & Kifonidis, K. 2003, Phys. Rev. Lett., 90, 241101

[17] Clayton, D. 1983, *Principles of Stellar Evolution and Nucleosynthesis* (Chicago: University of Chicago Press)

[18] Clocchiatti, A., Wheeler, J. C., Benetti, S., & Frueh, M. 1996a, ApJ, 459, 547

[19] Clocchiatti, A., Wheeler, J., Brotherton, M., Cochran, A., Wills, D., Barker, E., & Turatto, M. 1996b, ApJ, 462, 462

[20] Clocchiatti, A., et al. 1997, ApJ, 483, 675

[21] Clocchiatti, A., et al. 2000, ApJ, 529, 661

[22] Clocchiatti, A., et al. 2001, ApJ, 553, 886

[23] Dermer, C. 2004, astro-ph/0404608

[24] Drozdovsky, I., Schulte–Ladbeck, R., Hopp, U., Greggio, L., & Crone, M. 2002, AJ, 124, 811

[25] Feldmeier, J., Ciardullo, R., & Jacoby, G. 1997, ApJ, 479, 231

[26] Filippenko, A. 1987, IAUC4428

[27] Filippenko, A. 1988, AJ, 96, 1941

[28] Filippenko, A., Porter, A., & Sargent, W. 1990, AJ, 100, 1575

[29] Foley, R., et al. 2003, PASP, 115, 1220

[30] Freedman, W., et al. 2001, ApJ, 553, 47

[31] Galama, T., Vreeswijk, P., Pian, E., Frontera, F., Doublier, V., & Gonzalez, J. 1998, IAUC6895

[32] Galama, T., et al. 1999, A&AS, 138, 465

[33] Gal–Yam, A., Ofek, E., & Shemmer, O. 2002 MNRAS, 332L, 73

[34] Garnavich, P., Matheson, T., Olszewski, E. W., Harding, P., & Stanek, K. Z. 2003, IAUC8114

[35] Grothues, H. G., & Schmidt–Kaler, T. 1991, A&A, 242, 357

[36] Hamuy, M., et al. 2002, AJ, 124, 417

[37] Harkness, R., et al. 1987, ApJ, 317, 355

[38] Hatano, K., Branch, D., Nomoto, K., Deng, J. S., Maeda, K., Nugent, P., & Aldering, G. 2001, BAAS, 198, 3902

[39] Iben, I. 1967, ARA&A, 5, 571

[40] Iwamoto, K., et al., 2000, ApJ, 534, 660

[41] Jeffery, D. 1999, astro-ph/9907015

[42] Jha, S., Garnavich, P., Challis, P., & Kirshner, R. 1998, IAUC7011

[43] Kantowski, R., Kao, J., & Thomas, R. C. 2000, ApJ, 545, 549

[44] Kinugasa, K., et al. 2002, ApJ, 577L, 97

[45] Klose, S., Guenther, E., & Woitas, J. 2002, GCN, 1248, 1

[46] Korth, S. 1991, IAUC5234

[47] Korth, S. 1991, IAUC5251

[48] Krisciunas, K., & Rest, A. 2000, IAUC7382

[49] Kulkarni, S., Bloom, J., Frail, D., Ekers, R., Wieringa, M., Wark, R., & Higdon, J. 1998, IAUC6903

[50] Leibundgut, B., Phillips, M. M., & Graham, J. A. 1990, PASP, 102, 898

[51] Leibundgut, B., Tammann, G. A., Cadonau, R., & Cerrito, D. 1991, A&AS, 89, 537

[52] Lewis, J., et al. 1994, MNRAS, 266, L27

[53] MacFadyen, A. & Woosley, S. 1999, ApJ, 524, 262

[54] MacFadyen, A., Woosley, S. & Heger, A. 2001, ApJ, 550, 410

[55] Matheson, T., Filippenko, A., Chornock, R., Leonard, D., & Li, W. 2000, AJ, 119, 2303

[56] Matheson, T., Filippenko, A., Li, W., Leonard, D., & Shields, J. 2001, AJ, 121, 1648

[57] Maza, J., & Ruiz, M.T. 1989, ApJS, 69, 353

[58] Mazzali, P., Iwamoto, K., & Nomoto, K. 2000 ApJ, 545, 407

[59] Mazzali, P., et al. 2002, ApJ, 572, L61

[60] Mazzali, P., et al. 2003, ApJ, 599, L95

[61] McKenzie, E., & Schaefer, B. 1999, PASP, 111, 964

[62] Monard, B. 1998, IAUC6903

[63] Nakamura, T., Mazzali, P., Nomoto, K., & Iwamoto, K. 2001, ApJ, 550, 991

[64] Nomoto, K., Filippenko, A., & Shigeyama, T. 1990, A&A, 240, L1

[65] Pandey, S., Anupama, G., Sagar, R., Bhattacharya, D., Sahu, D., & Pandey, J. 2003, MNRAS, 340, 375

[66] Patat, F., Benetti, S., Cappellaro, E., Danziger, I. J., della Valle, M., Mazzali, P. A., & Turatto, M. 1996, MNRAS, 278, 111

[67] Patat, F., et al. 2001, ApJ, 555, 900

[68] Phillips, M. M., & Graham, J. A. 1984, IAUC3946

[69] Phillips, M., & Hamuy, M. 1992, IAUC5574

[70] Porter, A., & Filippenko, A. 1987, AJ, 93, 1372

[71] Poznanski, D., Gal-Yam, A., Maoz, D., Filippenko, A., Leonard, D., & Matheson, T. 2002, PASP, 114, 833

[72] Pun, C., et al. 1995, ApJS, 99, 223

[73] Qiu, Y., Li, W., Qiao, Q., & Hu, J. 1999, AJ, 117, 736

[74] Sollerman, J., Kozma, C., Fransson, C., Leibundgut, B., Lundqvist, P., Ryde, F., & Woudt, P. 2000, ApJ, 537, L127

[75] Richardson, D. 2001, Master Thesis, University of Oklahoma

[76] Richardson, D., Branch, D., Casebeer, D., Millard, J., Thomas, R. C., & Baron, E. 2002, AJ, 123, 745 (R02)

[77] Richmond, M., Treffers, R., Filippenko, A., Paik, Y., Leibundgut, B., Schulman, E., Cox, C. 1994, AJ, 107, 1022

[78] Richmond, M., et al., 1996, AJ, 111, 327

[79] Saha, A., Sandage, A., Tammann, G. A., Dolphin, A. E., Christensen, J., Panagia, N., & Macchetto, F. D. 2001, ApJ, 562, 314

[80] Schaefer, B. 1995, ApJ, 450, L5

[81] Schaefer, B. 1996, ApJ, 464, 404

[82] Schlegel, D., Finkbeiner, D., & Davis, M. 1998, ApJ, 500, 525

[83] Schlegel, D., & Kirshner, R. 1989, AJ, 98, 577

[84] Shigeyama, T., Nomoto, K., Tsujimoto, T., Hashimoto, M. 1990, ApJ, 361, L23

[85] Stritzinger, M., et al. 2002, AJ, 124, 2100

[86] Tsvetkov, D. 1985, Astron. Ah., 62, 365

[87] Tsvetkov, D. 1986, Sov. Astron. Letters, 12, 328

[88] Tsvetkov, D. 1994, Astronomy Reports, 38, 74

[89] Tully, R. B. 1988, *Nearby Galaxies Catalog* (Cambridge: Cambridge University Press)

[90] Turatto, M., Benetti, S., & Cappellaro, E. 2002, *From Twilight to Highlight – The Physics of Supernovae*, ESO/MPA/MPE Workshop Garching, ed. W. Hillebrandt & B. Leibundgut (Berlin: Springer), p. 200

[91] van Driel, W., et al. 1993, PASJ, 45, L59

[92] Vietri, M., & Stella, L. 1998, ApJ, 507, L45

[93] Wellmann, P., & Beyer, M. 1955, Z.Astrophysics, 35, 205

[94] Woosley, S., Eastman, R., & Schmidt, B. 1999, ApJ,516, 788

[95] Wheeler, J. C., & Levreault, R. 1985, ApJ, 294, L17

[96] Young, T., Baron, E., & Branch, D. 1995, ApJ, 449, L51

[97] Yoshii, Y., et al. 2003, ApJ, 592, 467

[98] Zeh, A., Klose, S., & Hartmann, D. 2003, astro-ph/0311610

Appendix A

Derivation of the Two–Filter K–Correction

The purpose of a K–correction is to compare the "y" magnitude of a redshifted object (spectrum) to an "x" magnitude of an object (spectrum) which is not redshifted.

$$K_{xy} = m_y - M_x - \mu \tag{A.1}$$

The distance modulus is $\mu \equiv 5log_{10}(D_L/10pc)$; where the luminosity distance, D_L, is in parsecs.

The equation for the observed apparent magnitude in Equation A.1 is given by:

$$m_y = -2.5log_{10}\Big[\frac{\int f(\lambda_o)S_y(\lambda_o)d\lambda_o}{\int \mathcal{Z}(\lambda_o)S_y(\lambda_o)d\lambda_o}\Big] + ZP_y. \tag{A.2}$$

$f(\lambda)$ = Spectrum of the object,

$S_y(\lambda)$ = Filter function for the "y" band,

$\mathcal{Z}(\lambda)$ = Spectrum of Vega,

ZP_y = Vega zero point for the "y" band,

o = observed frame,

e = emitted frame.

The absolute magnitude, M, is related to the luminosity density, $f(\lambda) = L(\lambda)/(4\pi D_L^2)$. The absolute magnitude is also the same as the apparent magnitude at a distance of 10pc. Using this and Equation A.2 we can write down the absolute magnitude (in the emitted frame) of Equation A.1.

$$M_x = -2.5log_{10}\left[\frac{\int \frac{L(\lambda_e)}{4\pi(10pc)^2} S_x(\lambda_e)d\lambda_e}{\int \mathcal{Z}(\lambda_e)S_x(\lambda_e)d\lambda_e}\right] + ZP_x \tag{A.3}$$

To convert the luminosity back to the flux we use the general equation: $L(\lambda) = 4\pi D_L^2 f(\lambda)$.

$$\begin{aligned} M_x &= -2.5log_{10}\left[\frac{\int \frac{4\pi D_L^2}{4\pi(10pc)^2} f(\lambda_e)S_x(\lambda_e)d\lambda_e}{\int \mathcal{Z}(\lambda_e)S_x(\lambda_e)d\lambda_e}\right] + ZP_x \\ &= -2.5log_{10}\left[\frac{\int f(\lambda_e)S_x(\lambda_e)d\lambda_e}{\int \mathcal{Z}(\lambda_e)S_x(\lambda_e)d\lambda_e}\right] - 2(2.5)log_{10}\left(\frac{D_L}{10pc}\right) + ZP_x \end{aligned} \tag{A.4}$$

Flux in the observed frame is related to flux in the emitted frame by: $f(\lambda_e)d\lambda_e = f(\lambda_o)d\lambda_o$, where $\lambda_o = (1+z)\lambda_e$. From this we have $f(\lambda_e) = (1+z)f(\lambda_o)$. Because Vega is nearby, however, we have $\mathcal{Z}(\lambda_e) = \mathcal{Z}(\lambda_o)$; and the same for the Vega zero points, ZP. We can now convert our apparent magnitude of Equation A.2 from the observed frame into the emitted frame.

$$\begin{aligned} m_y &= -2.5log_{10}\left[\frac{\int \frac{f(\lambda_e)}{(1+z)} S_y((1+z)\lambda_e)(1+z)d\lambda_e}{\int \mathcal{Z}(\lambda_e)S_y(\lambda_e)d\lambda_e}\right] + ZP_y \\ &= -2.5log_{10}\left[\frac{\int f(\lambda_e)S_y((1+z)\lambda_e)d\lambda_e}{\int \mathcal{Z}(\lambda_e)S_y(\lambda_e)d\lambda_e}\right] + ZP_y \end{aligned} \tag{A.5}$$

Putting all of this together we can calculate the K–correction.

$$\begin{aligned} K_{xy} &= m_y - M_x - \mu \\ &= -2.5log_{10}\left[\frac{\int f(\lambda_e)S_y((1+z)\lambda_e)d\lambda_e}{\int \mathcal{Z}(\lambda_e)S_y(\lambda_e)d\lambda_e}\right] + ZP_y \end{aligned}$$

$$+2.5log_{10}\Big[\frac{\int f(\lambda_e)S_x(\lambda_e)d\lambda_e}{\int \mathcal{Z}(\lambda_e)S_x(\lambda_e)d\lambda_e}\Big] - ZP_x$$
$$+2(2.5)log_{10}\Big(\frac{D_L}{10pc}\Big) - 5log_{10}\Big(\frac{D_L}{10pc}\Big) \qquad \text{(A.6)}$$

Canceling the last two terms and rearranging we get the final equation.

$$\begin{aligned} K_{xy} &= -2.5log_{10}\Big[\frac{\int \mathcal{Z}(\lambda_e)S_x(\lambda_e)d\lambda_e}{\int \mathcal{Z}(\lambda_e)S_y(\lambda_e)d\lambda_e}\Big] \\ &\quad + 2.5log_{10}\Big[\frac{\int f(\lambda_e)S_x(\lambda_e)d\lambda_e}{\int f(\lambda_e)S_y((1+z)\lambda_e)d\lambda_e}\Big] \\ &\quad -ZP_x + ZP_y \end{aligned} \qquad \text{(A.7)}$$